We fly as one

Design and Joint Control of a Conjoined Biplane and Quadrotor

Shawn Schröter

Faculty of Aerospace Engineering

We fly as one

Design and Joint Control of a Conjoined Biplane and Quadrotor

by

Shawn Schröter

to obtain the degree of Master of Science
in Aerospace Engineering
at the Delft University of Technology,
to be defended publicly on Friday March 11, 2022 at 9:30 AM.

Student number:	4492234	
Project duration:	September 1, 2020 – March , 2022	
Thesis committee:	Prof. dr. G.C.H.E. de Croon,	TU Delft, chair
	Dr. E.J.J. Smeur,	TU Delft, supervisor
	Ir. B. Remes,	TU Delft, supervisor
	Dr. K. Masania,	TU Delft, examiner
	Prof. dr. M. Voskuijl,	NLDA, external member

An electronic version of this thesis is available at http://repository.tudelft.nl/.

TU Delft

Preface

This thesis report concludes a 2.5-year adventure in Delft. While the first half of the academic year 2019/2020 looked promising, the pandemic quickly turned my perspective around. I had to find out the hard way that studying from your study room without many social interactions is very difficult. However, here we are, and I could not have done this alone.

First, I would like to thank my supervisors for the proper guidance. Ewoud, you are one of the most patient mentors I have had so far. Your knowledge is spot on, and you have really helped me reach a higher academic thinking level. Bart, thank you for asking the right questions during my research process and helping me with the practical tests when I needed it the most.

Second, I would like to thank the members of the MAVlab. Freek, thank you for helping me with all the practical tests as the second pilot, but also for all of the fun talks we had during work. Dennis, thank you for also helping me out with all the practical tests and coding of the flight controller. It was really nice that we both had our own project, but could help each other out in such an effective manner. Mathieu and Nicholas, thank you for helping out with the initial work on the release mechanism and your awesome work bringing the aircraft alive in Solidworks. But also Eric, Jack, Tomaso and Pietro, and the other members of the MAVlab, I had heaps of fun working with you.

Thirdly, I would like to thank my friends. I have not always been the easiest to be around during the constant pressure of the thesis, but I have always felt your support. Guillermo, Memo, without our endless study sessions together, I would not have finished my MSc. anywhere close to this time frame. Your constant support shows that you are a true friend.

And lastly, I would like to thank my family. My dad, my mom, and my sister, Thank you for always listening to me. This adventure in Delft has been a roller-coaster, and thank you for your unconditional support in whatever choices I made.

Onto the next adventure. Sky is the limit!

Shawn Schröter
Delft, March 2022

Abstract

Unmanned Aerial Vehicles, UAVs, serve many purposes these days, such as short-range inspections and long-distance search and rescue missions. Long-distance missions can entail a search in a building. Such missions require a large aircraft for endurance and a small aircraft for manoeuvrability in a building.

This work proposes a novel combination of a quadrotor and a hybrid biplane capable of joint hover, joint forward flight, and mid-air disassembly followed by separate flight. During joint flight, the quadcopter and the biplane have no intercommunication.

This works covers the design of a release system and a joint control strategy. Firstly, the in-flight release is successfully tested in joint hover up to a forward pitch angle of -18 [deg]. Secondly, three control strategies for the quadrotor are compared: a proportional angular rate damper, a proportional angular acceleration damper, and constant thrust without attitude control. In all cases, the biplane uses a cascaded INDI attitude controller. Simulation and practical tests show that for intentional attitude changes, the different strategies are of minimal influence. However, the angular rate damper strategy for disturbance rejection has the lowest roll angle error and requires the smallest input command.

Contents

List of Figures

1 Introduction

1.1. Background

A little over a hundred years ago, the Wright brother invented the first motorized aircraft. Since then, developments in the field have literally taken flight. A relatively recent innovation is formed by Unmanned Aerial Vehicles, UAVs, and the past decade has seen their popularity increase quickly. UAVs are ideal for inspection of structures or for traffic management during events, but they can also assist in medical emergencies. UAVs come in all shapes and sizes. Fixed-wing aircraft are known for their endurance and efficiency, but they require a constant horizontal speed to stay in the air. Multirotors are more agile and are capable of hover, but they lack endurance. A hybrid aircraft combines the best of both worlds. These aircraft can hover and usually have stationary wings, which makes the aircraft highly efficient in forward flight. Imagine a situation where the goal is twofold: to perform a long-distance transit flight and to manoeuvre inside a building. This need could arise if, for example, an aircraft has to provide situational awareness in an unapproachable building. Here, a combination of endurance, efficiency, and a small size would be required. One could say that the hybrid aircraft would answer this need, but the long-distance aircraft that would be required for such a task would likely be too big. In order to meet the physical requirements, a novel combination is developed: a combination of a biplane and a quadrotor. This joint structure is illustrated in Figure 1.1. The bigger structure, the biplane, is a hybrid biplane and the smaller structure is a quadrotor.

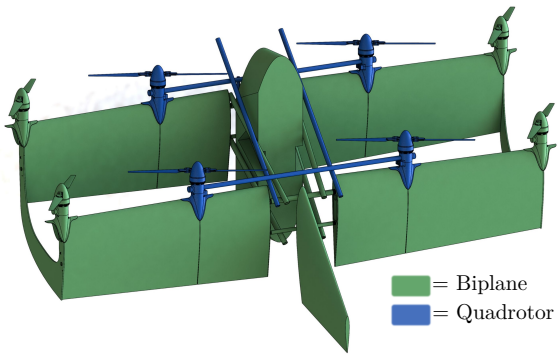

Figure 1.1: The joint structure. It consists of a hybrid biplane, coloured in green, and a quadrotor, coloured in blue.

The two aircraft shown above would take off together, fly in forward flight together, transition back to a hover state, and **disassemble in-flight**. The smaller UAV would then manoeuvre into a building, and the fixed-wing aircraft would loiter above the building to function as a data relay station. Figure 1.2 shows the different phases of the joint structure's activities. Since most of these actions have never been performed before, academic research needs to be performed to tackle these problems. This thesis discusses feasible solutions to some of the challenges facing the new joint structure. Its main

objective is to design a reliable control strategy for both a multirotor and a biplane, by analysing flight behaviour during manual test flights. Both platforms should contribute to flight when necessary, giving both the endurance of the biplane and the eventual agility of the later released multirotor. Both aircraft are not allowed to communicate with each other.

(a) Joint Hover

(b) Joint Forward flight

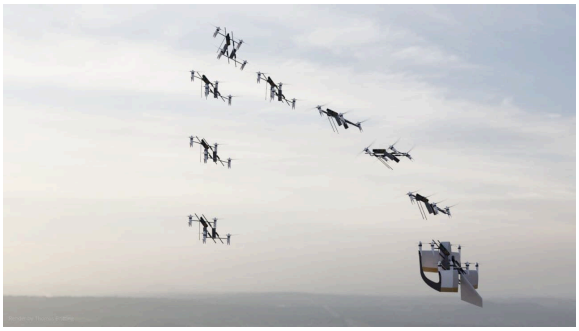

(c) In-flight release

(d) The quadrotor manoeuvring in a building, while the biplane loiters (in forward flight) as a data relay station

Figure 1.2: Different phases of the joint structure's activities

1.2. Research Aim

The current thesis aims to answer the question how rigidly interconnected flying vehicles can be controlled without communication between them and with the possibility of mid-air disassembly. To this end, the main research question is divided into a number of sub-questions:

1. How can a multirotor interconnecting with a VTOL biplane be designed with the ability of in-air disassembly?
2. What is a robust control strategy for two interconnected aircraft without intercommunication?
   (a) What type of control method has been used for cooperative aircraft?
   (b) What type of communication is used in cooperative flight?
   (c) What constraints are created if no intercommunication exist?
   (d) What type of decision making role should exist between two interconnected vehicles that have no intercommunication?
   (e) What kind of control is required for a hybrid aircraft during its different phases of flight?
   (f) What type of control strategy should be implemented for two interconnected vehicles without intercommunication during hover?

1.3. Report outline

Following the introduction of our research aim and research questions, in Part I our research objective is considered and the main research question is answered. This is done in the form of a scientific paper. This paper can be considered as a self-standing document. Part II of this thesis presents a literature review to determine which of the research questions have already been answered, either in full or in part. Chapter 2 outlines different types of aircraft, with a main focus on their control. Chapter 3 then discusses the different theoretical ways of controlling an aircraft. Chapter 4 covers various forms of multiple aircraft flying together, ranging from physically connected aircraft to formation flight and the in-flight disassembly of multiple aircraft. Chapter 5 discusses which research questions can already be (partly) answered and what still remains to be investigated. This research gap then forms the basis for the remainder of the thesis report. Part III of this manuscript presents preliminary and additional research results. Finally, part IV presents the conclusion and recommendations.

I

Scientific Paper

Design and Joint Control of a Conjoined Biplane and Quadrotor

Shawn Schröter
Delft University of Technology, 2629 HS, the Netherlands

***Abstract*—Unmanned Aerial Vehicles, UAVs, serve many purposes these days, such as short-range inspections and long-distance search and rescue missions. Long-distance missions can entail a search in a building. Such missions require a large aircraft for endurance and a small aircraft for manoeuvrability in a building.**

This paper proposes a novel combination of a quadrotor and a hybrid biplane capable of joint hover, joint forward flight, and mid-air disassembly followed by separate flight. During joint flight, the quadcopter and the biplane have no intercommunication.

This paper covers the design of a release system and a joint control strategy. Firstly, the in-flight release is successfully tested in joint hover up to a forward pitch angle of -18 [deg]. Secondly, three control strategies for the quadrotor are compared: a proportional angular rate damper, a proportional angular acceleration damper, and constant thrust without attitude control. In all cases, the biplane uses a cascaded INDI attitude controller. Simulation and practical tests show that for intentional attitude changes, the different strategies are of minimal influence. However, the angular rate damper strategy for disturbance rejection has the lowest roll angle error and requires the smallest input command.

***Index Terms*—in-flight release, joint flight, tailsitter, quadrotor, hybrid biplane, INDI**

I. Introduction

Unmanned Aerial Vehicles, UAVs, have increased in popularity and can serve various purposes, ranging from inspection of structures to traffic surveillance, and each type of UAV has its own distinguishing properties. Fixed-wing aircraft are known for their endurance and efficiency, but they require a constant horizontal speed to stay in the air. Multirotors are more agile and are capable of hover, but they lack endurance. A hybrid aircraft combines the best of both worlds. These aircraft can hover and usually have stationary wings, which makes the aircraft highly efficient in forward flight. Imagine a situation where the goal is twofold: to perform a long-distance transit flight and to manoeuvre inside a building. This need could arise if, for example, an aircraft has to provide situational awareness in an unapproachable building. Here, a combination of endurance, efficiency, and a small size would be required. One could say that the hybrid aircraft would answer this need, but the long-distance aircraft that would be required for such a task would likely be too big.

One solution aimed at achieving the above-mentioned two-fold goal is to drop a smaller UAV out of a bigger one. For in-flight release, multiple options exist. Examples include a quadrotor dropping a fixed-wing UAV[1] and morphing UAVs being dropped as armaments out of (military) airplanes [1]. In all of these in-flight release cases, the propulsion of one of the aircraft would not be utilised when the two aircraft are (physically) together. This means that part of the available propulsion is not used at any given time during flight. Usually, the weight of the smaller aircraft is carried around as dead weight; however, when endurance is a factor that needs to be optimised, carrying around dead weight has adverse effects.

Another solution could be a form of cooperative flight: this is when two aircraft each perform propulsion during transit. Cooperative flight can be subdivided into formation flight, where individual aircraft do not form a physical connection [2], and flight with modular joint airframes, where physical connections exist between the different aircraft [3]–[5].

Various forms of control theories have been proposed for formation flights with UAVs [6]–[11]. Conventional formation flights have one aircraft as the flight leader, with the others flying their trajectory relative to the flight leader [12]. Swarming is another form of formation flight. Here the trajectory can be determined by either a virtual flight leader [13], or the trajectory is partly determined by the relative position to their neighbours [8], [9]. These types of cooperative flight, however, have not yet been investigated extensively enough when it comes to combining long-distance flight and an ability to manoeuvre inside a building.

In terms of practical verification for formation flight, centralised control is often used. This means that a ground computer makes calculations aiding the formation in control. Decentralised formation flights have also been demonstrated, but data communication for formation control is mentioned as a liability [8], [14], [15]. In particular, time delay, noise, and false information can result in aircraft making control decisions based on incorrect data.

Examples of cooperative flight with modular joint airframes are the Modquad and the Distributed Flight Array [3], [4]. Both airframes are capable of assembling in-flight, and the latest version of the Modquad is even capable of in-flight disassembly [16]. However, all aircraft used in this research have the same size, and endurance has not been mentioned.

For a UAV's attitude and trajectory control specifically, many options exist. The most popular method is PID control [17], but also model-based controllers exist for UAVs [18].

Email address: s.schroter@student.tudelft.nl

[1] https://www.boeing.com/features/2016/09/catch-and-release-flares-09-16.page

For hybrid aircraft, Incremental Nonlinear Dynamic Inversion, INDI, has proven to be very effective [19]. Especially in the hover phase, hybrid aircraft are extremely susceptible to external disturbances [20], and INDI has better disturbance rejection compared to PID [21].
In order to meet the physical requirements, a novel combination is developed: a combination of a biplane and a quadrotor. This joint structure is illustrated in Figure 1. The bigger structure, the biplane, is a hybrid biplane and the smaller structure is a quadrotor.

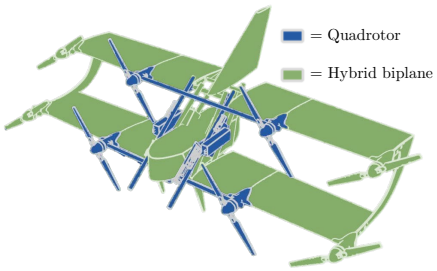

Fig. 1: The joint structure. It consists of a hybrid biplane, coloured in green, and a quadrotor, coloured in blue.

The two aircraft of different sizes cooperatively take off vertically, transition to forward flight, and fly in transit. On location, these aircraft will transition back to hover, then disassemble in-flight, and the smaller aircraft would be able to manoeuvre inside a building. Figure 2 graphically shows the various stages in which the joint structure would fly.

As mentioned above, different forms of communication have been used in all forms of cooperative flight between different aircraft, but this has proven to have its challenges, such as time delays, false information and noise. Wired communication between the aircraft would be less of a liability, but a way to work around all these problems is to avoid any communication altogether. That is why a control strategy is proposed in this paper where both aircraft have no communication with each other. This way, the joint structure becomes more reliable, which is very important for long-distance operations.

Two main questions will be dealt with: how can the joint vehicle be controlled and how can the two aircraft be disassembled in mid-air?

The paper is structured as follows: first, in Section II a physical description is given of the joint structure. Next, in Section III and IV parameters are defined that are necessary to properly analyse the joint structure and to argue what control strategy seems most feasible. Section V presents three different control strategies for the quadrotor: Constant Thrust, Angular Rate Damper and Angular Acceleration Damper. The control group strategy will also be discussed in this section. Simulation results in terms of step responses and theoretical stability analysis will be covered in Section VI. Practical verification will show that each aircraft can individually fly, the in-flight release is covered, and the joint control strategy results for hover are covered in Section VII. Lastly, the conclusion and discussion are presented in Sections VIII and IX.

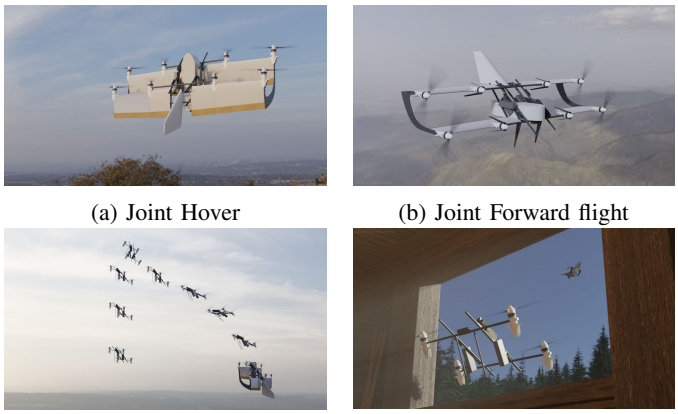

(a) Joint Hover

(b) Joint Forward flight

(c) In-flight release

(d) The quadrotor manoeuvring in a building, while the biplane loiters (in forward flight) as a data relay station

Fig. 2: Different phases of the joint structure's activities

II. Joint Structure Design

Figure 2 shows the joint structure in its various flight configurations, and this section will cover three main parts of the structure in more detail; The hybrid biplane, the quadrotor and the release mechanism.

A. Hybrid biplane

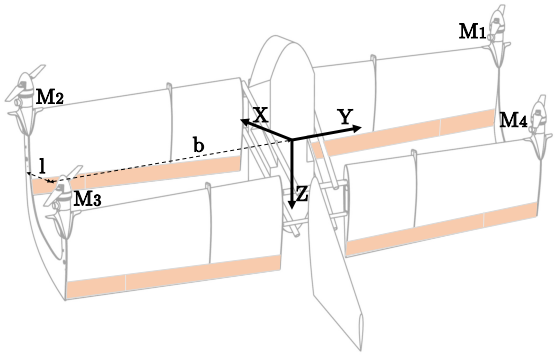

Fig. 3: Schematic drawing of the hybrid biplane and axis definitions, with the control surface accentuated in light orange. M_i illustrates the ith rotor actuators.

The biplane is a tailsitter hybrid aircraft. For this aircraft, the Nederdrone formed the basis of the biplane design [19]. The biplane has eight mounting points for rotors and four control surfaces. The four outer mounting points are fixed, and the four inner mounting points are part of the release mechanism. The control surfaces control the airflow around the wings, providing moments around the Y- and Z-axes. In the hover phase, this airflow is created by the rotors. Table I presents an overview of the different parts of the hybrid

biplane. The reference frame is defined in hover state, a shown in Figure 3. Forward flight would mean a $-90°$ pitch angle.

TABLE I: Different components of the biplane

Type of Hardware	Brand	Item
Motor	T-Motor	MN3510
Radio Control link	TBS	Crossfire nano
Telemetry link	Herelink	Herelink
Electronic Speed Controller	T-Motor	f45A 32_bit
Propeller	T-motor	MF1302
Flight controller	Holybro	Pixhawk4
Battery	Extron	2x 6s 4.5 Ah

B. Quadrotor

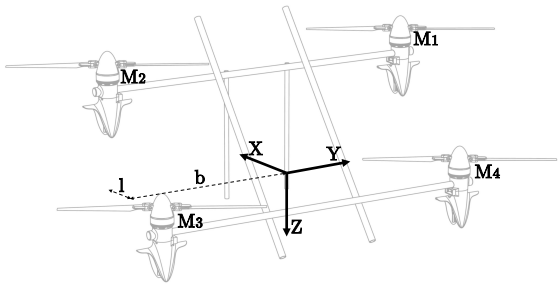

Fig. 4: Schematic drawing of the quadrotor, with axis definitions.

The design of the quadrotor is derived from the dimensions of the biplane. This means that on the four inner mounting points of the biplane the four rotors of the quadrotor are placed. In order to save weight, the frame had to be made as light-weight as possible but still be strong enough. Therefore, four hollow carbon rods connect the four rotors. The rods are placed in such a way that the quadrotor would be able to release without being obstructed by the biplane. A schematic overview of the quadrotor is shown in Figure 4. Figure 2c shows the release if the biplane is in hover. If the joint structure were to pitch forward significantly, i.e. to counteract the wind, the back propellers of the quadrotor could hit the biplane's wings before separation would be completed. In order to prevent this from happening, two solid carbon guiding tubes were implemented. These also function as landing legs. The powertrain is similar to the biplane. One difference is that the quadrotor uses two 3s 4500 mAh batteries, connected up in series. This then translates into one 6s 4500 mAh battery.

C. Release mechanism

The release mechanism is mounted just underneath the motors of the quadrotor. At each of the four motor locations, two copper pins hold the quadrotor attached to the biplane. The release system is a slider-crank mechanism. Here, the rotational energy comes from an Radio Controlled, RC, servo. Once the servo has been commanded to release by the quadrotor, it will translate its rotational energy to a straight-line motion of the pins.

The two biggest forces that apply to the release mechanism are the net weight of the biplane and the thrust of the quadrotor. These forces oppose each other and are both perpendicular to the pins. Since the pin and the release mechanism counteract the thrust force, the quadrotor's lift force is translated to the biplane.

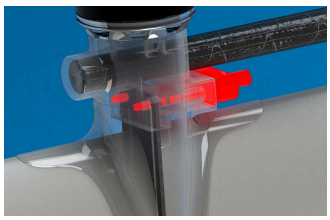

(a) Closed position - The pin is locked in the carbon plate.

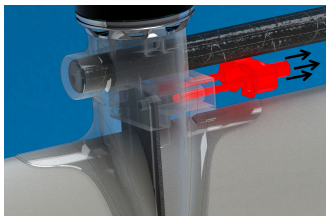

(b) Open position - The pin has moved inward, unlocking from the carbon plate.

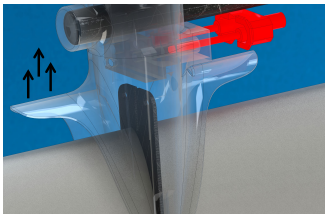

(c) Lift-off of the quadrotor

Fig. 5: Closed, open position and release of the RC servo Release Mechanism

Figure 5 shows graphically how the release system enables the quadrotor to separate from the biplane. Once the pins are out, the motor mount slides in the direction of the thrust force. A thrust difference between the tailsitter and the quadrotor then leads to separation. The guiding tubes of the quadrotor, mentioned in Section II-B, help the thrust force of the quadrotor to stay approximately opposite to the weight force of the biplane.

III. Model Structure

This section will explain how the aircraft models are defined to control the joint structure properly.

A. Control law

As mentioned in the Introduction, both aircraft will be flying in three different flight phases: joint hover, joint forward flight, and separate hover. A control law for both hover phases will need to be designed first, since joint forward flight can only be achieved after the joint hover phase is properly controlled.

For the flight control strategy, Incremental Nonlinear Dynamic Inversion, INDI, is chosen as a starting point. INDI has proven to perform very well for tailsitter hybrid aircraft. These aircraft have different aerodynamic properties during the different flight phases and are very sensitive to wind gusts in hover. INDI is robust and has good wind gust rejection [19]. INDI not only performs well with hybrid aircraft, but [21] has also proven that INDI has benefits in similar ways for quadrotors.

For both aircraft the following angular momentum equation holds:

$$M = I_v\dot{\Omega}+\Omega\times I_v\Omega = M_a(\Omega,v)+M_c(\omega)+M_r(\omega,\dot{\omega},\Omega) \quad (1)$$

where M is the total moment, I_v is the inertia around the rotational axis of the aircraft, ω is the angular rate of the propellers around the body Z-axis and $\dot{\omega}$ is the angular acceleration of the propellers around the body Z-axis. M_a is the moment due to aerodynamics, M_c is the moment due to the controls, M_r is the moment due to the gyroscopic effect of the rotors and Ω is the angular rotation vector.

Equation 1 can be used to derive the general control law of INDI, described as:

$$\omega_c = \omega_f + (G_1+G_2)^+(v-\dot{\Omega}_f + G_2 z^{-1}(\omega_c-\omega_f)) \quad (2)$$

where ω_c is the current motor command, ω_f is the motor command of the previous iteration, G_1 describes the control effectiveness of the actuators, G_2 describes the gyroscopic effect on the Z-axis, $\dot{\Omega}_f$ is the measured angular acceleration, and v is the virtual input. This virtual input is defined as the reference angular acceleration created by a PD controller. A full derivation is given in [22].

B. Control authority analysis

To analyse how the two aircraft compare considering control authority, the control moment from Equation 1 is used. Per axis, the control moment, M_c, is defined for a multirotor as [23]:

$$\boldsymbol{M_c} = \begin{bmatrix} -bk_1 & bk_1 & bk_1 & -bk_1 \\ lk_1 & lk_1 & -lk_1 & -lk_1 \\ k_2 & -k_2 & k_2 & -k_2 \end{bmatrix} \boldsymbol{\omega}^2 \quad (3)$$

where b is the lateral distance from the Centre of Gravity, CG, to the rotors, l is the longitudinal distance between the CG and the rotors, k_1 is the force constant of the rotors, k_2 is the moment constant of the rotors, and ω is the angular rate vector of the rotors.

From Equation 3 the control effectiveness of the different actuators can be derived. The force constants are the same for the biplane and the quadrotor, since the same hardware is used for both aircraft. If the control surfaces were negated, both the biplane and the quadrotor separately can be seen as two quadrotors, where 3 holds.

Figure 3 and 4 show an overview with the lateral and longitudinal distances. For roll, the distance b for the actuators of the biplane are more than twice as long than for the quadrotor. For pitch, the distances are the same, and for yaw the moment is created around the Z-axis and is therefore not dependent on either b or l. Table II shows an overview of b and l for the biplane and the quadrotor.

By comparing b and l in Table II, Equation 3 states that it is only around the roll axis the biplane has more control authority than the quadrotor. For pitch and yaw the control surfaces of the biplane aid in control. The airflow around the control surfaces is not constant throughout the flight profile, making it difficult to accurately determine the control effectiveness of the control surfaces at different thrust levels. However, these control surfaces do in fact aid the joint structure in attitude control. In conclusion, in all rotational directions the biplane has more control authority than the quadrotor.

TABLE II: lateral and longitudinal distances from rotor actuators to CG for the biplane and the quadrotor.

	b	l
Biplane	0.74 [m]	0.11 [m]
Quadrotor	0.32 [m]	0.11 [m]

IV. Control strategy of the joint structure

This section investigates the choices and constraints for the joint control strategy, given the physical choices mentioned earlier.

A. Measurements

In the previous section, INDI was selected as the global controller for the joint structure. Since the two aircraft have to disassemble and be capable of separate flight, two flight controllers must be run. The sensors for both aircraft consist of a three-axis accelerometer, three gyroscopes, a barometer, and a GPS. In order to determine what type of control each aircraft would need, the measured states of both aircraft were analysed.

The GPS is known to have an accuracy of approximately one meter, resulting in significant deviations between measurements of both aircraft. The barometer is not very accurate either, providing significant and changing deviations between measurements for the height.

For attitude measurements, a Kalman filter is applied to obtain a better estimation using sensor fusion. The Kalman filter fuses the measurements pretty well, but an angle deviation remains. One reason for this is the misalignment between flight controllers. Every time the two aircraft are connected together and turned on, they will calibrate their attitude state differently. However, the deviation is also not constant. This has other reasons, including different noise and bias levels of the sensors and the fact that the body of the joint aircraft is not completely rigid. A way to deal with this is to have both aircraft check each state and fuse the estimation together, but this would require intercommunication.

To a certain degree, some of the deviations can also be tackled by carefully calibrating the attitude angles of the quadrotor with respect to the biplane. However, this then has to be performed prior to every flight and should therefore be avoided if possible. Furthermore, during assembly of the two aircraft, the attitude states would not be completely the same, thus still resulting in an difference.

However, Figure 6a shows that the raw gyro measurements overlap quite well. The quadrotor has more noisy measurements than the biplane, but these deviations become smaller after the application of a Butterworth filter. This result can

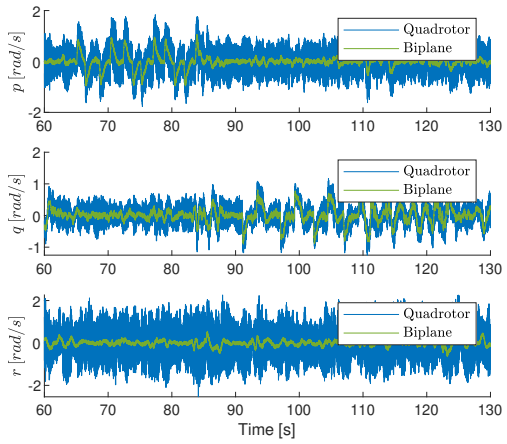

(a) Raw gyroscope measurements.

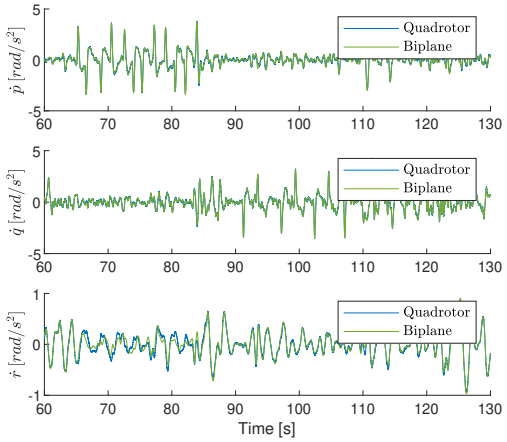

(b) Angular accelerations, purely derived from gyroscopes.

Fig. 6: Gyroscope measurements during a particular flight in joined hover. After filtering, the signals overlap quite well.

be seen in figure 6b. The angular acceleration values are derived by filtering the raw gyro measurements and taking the derivative. Now the difference between measurements is minimal. In conclusion, the gyroscope measurements provide the most similar data between the two flight controllers of the joint structure without intercommunication.

B. Reference states

Another critical part of designing a control strategy is to know what reference state should be used. Similar to what was done in the previous section, analyses are made in this section regarding the types of reference states that are available and reliable.

As a result of the lack of intercommunication, one of the two aircraft would not know the reference model. The reference states consist of 3-dimensional position waypoints during autonomous flight, alongside attitude states. An outer loop controller will calculate the desired attitude, and the inner loop controller tries to reach a zero track error to that desired attitude. In this case, the full attitude states are the roll, pitch, and yaw angles. It would be ideal for both aircraft to have an inner- and an outer control loop. GPS is used for position determination, but GPS is too inaccurate. The GPS measurement deviations would result in different attitude reference states, which generate different commands. This causes unnecessary input, decreasing the control authority. We can, therefore, not send both aircraft the waypoint commands.

Since the attitude is calculated using the waypoint references, it is also not possible to have both aircraft receive the attitude reference from a base station.

Another reason why only one aircraft would receive the waypoints is that, like interconnection, time delay and other connection hiccups can occur between a base station and the aircraft, again yielding different information for both aircraft.

Given all the previous constraints, the best option is to leave full knowledge of the reference states to just one aircraft, the biplane. The reason is that the biplane has relatively more control authority, as illustrated in Section III, and would therefore benefit more from it. The biplane will be controlled using the INDI control scheme. Note that in this paper only the inner attitude loop is covered. In formation flight terms, the biplane will behave like a leader in a formation flight, where the quadrotor will try to make its control decisions based on the behaviour of the biplane.

V. Control Strategies for the Quadrotor in Joint Hover

With the options considering measurements and the reference states known, the control strategy for the quadrotor is determined in this section.

The goal is to have the quadrotor improve the overall performance of the joint structure. Firstly, this means that the least amount of energy should be required to perform flight. Secondly, good step response and disturbance rejection behaviour is preferred. Tailsitter platforms, like the hybrid biplane, generally struggle with disturbance rejection in hover [20], [24]. One of the reasons is that in hover, the tailsitter can have the large aerodynamic surface be perpendicular to the wind. Furthermore, wind gusts are unpredictable and hard to model. Especially around the Z-axis, a tailsitter can require quite some control input to deal with disturbance rejection.

Thirdly, for command, the goal is always for it to be as small as possible. Less required input command means that the actuators are further away from their saturation point, giving the actuators more room for extra manoeuvring.

It is given that the quadrotor at least has to give a specific throttle command. Otherwise, the weight of the quadrotor cannot be counteracted. This is necessary especially in hover. The first investigated control strategy does just this. It gives a specific equal thrust command to all four quadrotor actuators. Basically, this follows the same principle as the Lunar Lander Research Vehicle in its 'gimbal fixed' configuration: a jet provides thrust to help without actively contributing to attitude control, while other actuators are responsible for attitude and the rest of the thrust [25]. Here, the quadrotor provides only

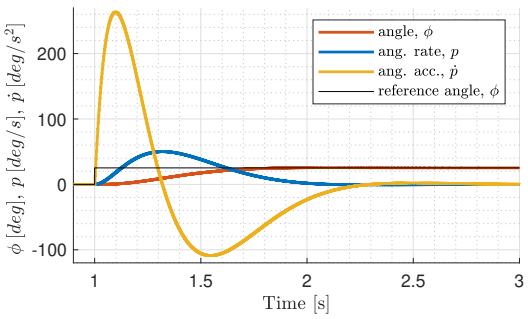

Fig. 7: Roll angle, angular rate and angular acceleration response after an intended step input. The angular rate and acceleration return to zero at the new steady state, whereas the roll angle has a constant nonzero value.

thrust and the biplane is responsible for the rest of the thrust as well as attitude control. This control strategy will be referred to in the remainder of the paper as *constant thrust*.

Since the biplane is given full knowledge of the reference frame and the quadrotor does not know the desired reference frame either from centralised control or the biplane, it has to develop its own. A major challenge is to distinguish the difference between intended change in attitude or an external disturbance changing the attitude. Intended behaviour is created by changing reference signals, stemming from an outer-loop position controller or manual input from an RC controller. In Section VII, the latter is used. Unintended behaviour is usually the result of external forces acting on the platform. This can be wind, thermals, or something breaking off the aircraft. Given an absence of intercommunication, and for simplicity's sake, the quadrotor will not need to differentiate between the two and will see both occurrences as a disturbance.

If the quadrotor sees every movement as a disturbance, it will try to counteract every movement that the joint structure is making. If the quadrotor uses a full attitude controller, it will constantly try to counteract the angles that the biplane tries to achieve. For example, if the biplane is in hover and has to counteract wind, it must maintain a certain non-zero pitch angle. This causes the quadrotor flight controller to measure a constant offset. Both INDI and PID yield an integrating component that will keep increasing the input command every time an error exists. This would cause unnecessary saturation on the rotors. A mere PD controller is not feasible either, since this does not solve the measured deviation caused by the biplane. In conclusion, the full attitude states are not feasible for reference.

Figure 7 shows the behaviour of the angle, the rotational rate and acceleration after a step input.

If the aircraft transitions from one angle to another, both the rotational rate and acceleration are non-zero during the transition. However, the angular rate and acceleration are zero during steady-state in the beginning and at the new steady-state angle. Also, as mentioned in Section IV-A, both flight controller measurements align well with angular rate and angular acceleration, but not for attitude angles. This indicates that rotational rate and angular acceleration could be used as a zero reference for any given steady-state attitude angle of the joint structure.

The next two investigated strategies will use either the angular rate or the angular acceleration to keep a zero reference. The type of control will be proportional control. These strategies will be referred to as *angular rate damper* and *angular acceleration damper*. Figure 8 shows the block diagrams for the three strategies. With the damper strategies, both the biplane and the quadrotor will detect a disturbance and will try to steer against this. In this way, the quadrotor is helping the biplane counteract the disturbance. However, with both damper strategies, the quadrotor will also detect the intended behaviour of the biplane as a disturbance. If the damper strategies need to improve the overall performance of the joint structure, the performance gain in disturbance rejection has to outweigh the loss in the intended behaviour.

A. Control group for base reference

In order to compare the effect of control strategies from the quadrotor, performance has to be tested against a base reference. This base reference is one INDI attitude controller directly controlling *all eight rotor actuators and the control surfaces*. This makes the control group physically different from the three investigated control strategies for the quadrotor. For this strategy to work, the motors of the quadrotor are directly wired to the Electronic Speed Controllers and the flight controller of the biplane. This implies another control effectiveness compared to cooperative control, and this is taken into account for Section VII. In the next sections this base reference is referred to as the *control group*.

VI. Simulation

In this section, the developed controllers are implemented into MATLAB Simulink. The INDI controller of the biplane is simulated as mentioned in [27]. The joint controller is simulated as a rigid body, meaning that the dynamics of both aircraft can be summed up. Because simulation is used to verify the working principles, it has been simplified. The goal is not to have the simulations perfectly approximate reality. The overview of the control loop is given in Figure 8. For simulation, only the roll axis is simulated. Around the roll axis, the control surfaces of the biplane are of no use. Since these control surfaces are more difficult to model accurately, rotations around the roll axis yield a better approximation to practical verification.

To analyse flight performance of the joint structure in hover, the behaviour of the aircraft is divided into intended and unintended behaviour. Intended and unintended behaviour happen in real flight at different rates (frequencies) and at different amplitudes. Step inputs are created for both types of behaviour to compare the different strategies. In this way, a real stochastic flight profile can be developed via deterministic occurrences. The intended step input is created by increasing the reference state and the step disturbance is created by

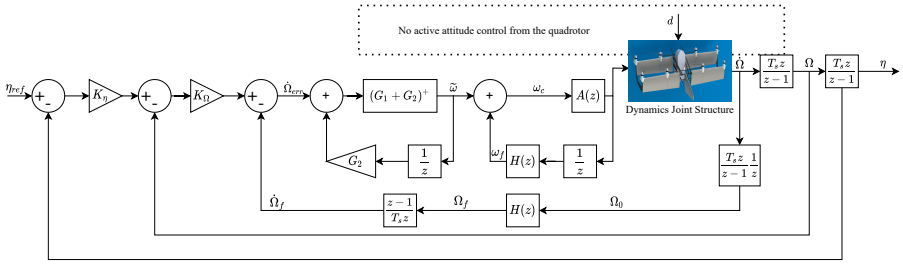

(a) Strategy 1 - Constant thrust

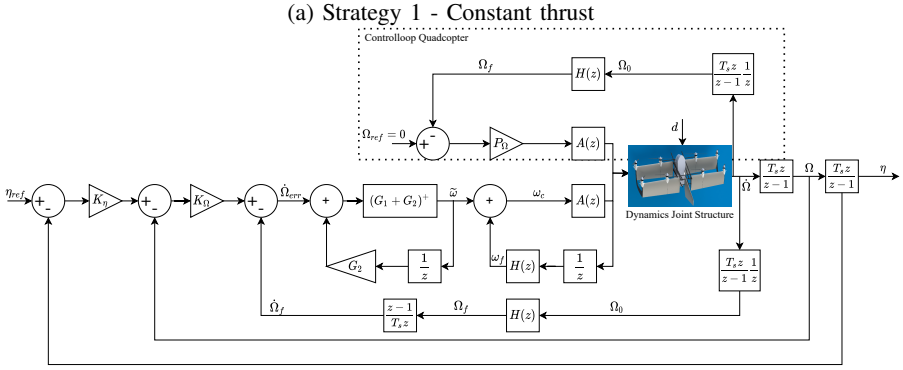

(b) Strategy 2 - Angular rate damper

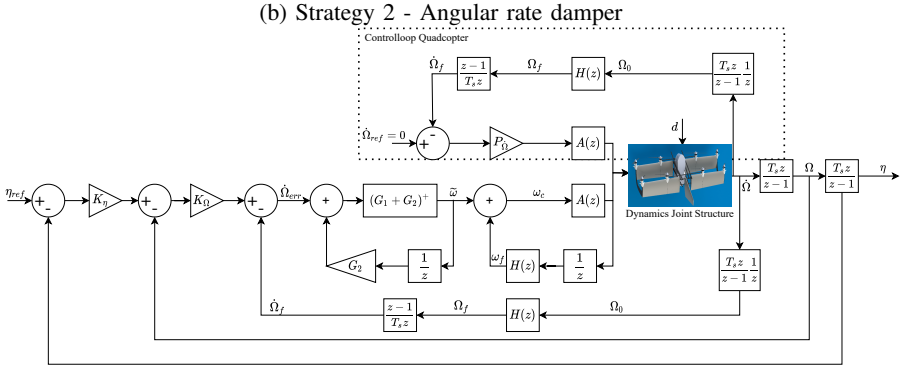

(c) Strategy 3 - Angular acceleration damper

Fig. 8: Three control strategies for the quadrotor. The lower section of the loop shows the INDI cascaded attitude controller of the biplane. The area within the dotted line resembles the control loop for the quadrotor.

adding a moment to the joint structure dynamics block. This disturbance is illustrated by d in Figure 8.

For both simulation and the practical verification, the input command is scaled by the definitions of the Paparazzi UAV autopilot [28]. For roll, pitch, and yaw, the command limits are set from -4500 to 4500 and for thrust the command ranges from 0 to 9600. The unit of this scaled input command is defined as [PPRZ].

A. *Matlab Simulations on the different control strategies*

In order to quantify how good the intended step input response is, the plots are analysed using overshoot and settling time. For settling time error bands are set to 5% of the final value [29]. Also, the input command needed for the biplane to perform the movement is quantified. The total input command is also considered to determine the amount of energy required to perform the step input. Note that this is an approximation of the actual amount of energy required. In reality power consumption relies on more factors than the total input command. Table III and IV displays an overview of these parameters for the strategies. Figure 9 and 10 show the responses visually.

The roll angle for constant thrust has a very minimal overshoot, not even crossing the error band for the settling time. The control group has the exact same response. This is due to the nature of the INDI controller. Closed-loop analysis shows that the response is more dependent on the PD outer-loop gains and the actuator dynamics than the control effectiveness [22]. However, a significant difference in the roll command exists, as shown in Figure 9b. The positive input command for the control group has a significantly lower value compared to the other three strategies. The maximum required input values for the other three strategies are all rather similar. When the joint structure is nearing the new steady state, the angular

TABLE III: simulation results for the different strategies for an intended step input. Based on simulation, the angular rate damper strategy is expected to have the least energy required for an step input, while having a little less performance.

	Settling time	**Overshoot**	**Max. input command**	**Energy required for t=[0-5]**
control group	1.40 [sec]	1.47 [%]	383 [PPRZ]	148 [PPRZ· s]
ang. rate damper	1.82 [sec]	5.95 [%]	480 [PPRZ]	139 [PPRZ· s]
constant thrust	0.76 [sec]	1.47 [%]	478 [PPRZ]	185 [PPRZ· s]
ang. acc. damper	0.76 [sec]	9.52 [%]	488 [PPRZ]	255 [PPRZ· s]

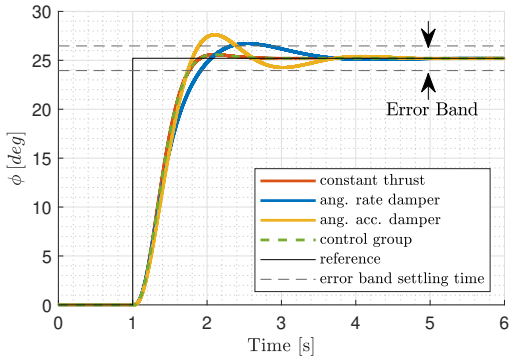

(a) Roll angle after intended Step input

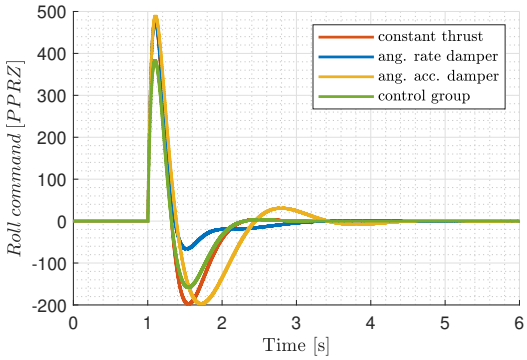

(b) Roll input command after intended Step input

Fig. 9: Intended step input behavior in the Hover phase.

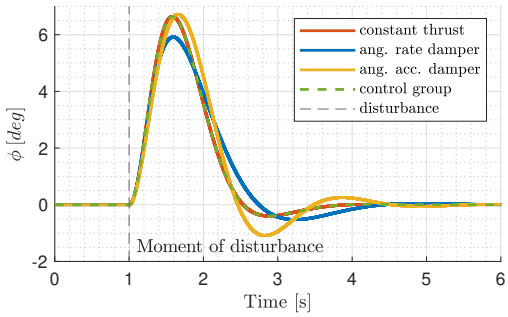

(a) Roll angle for disturbance rejection

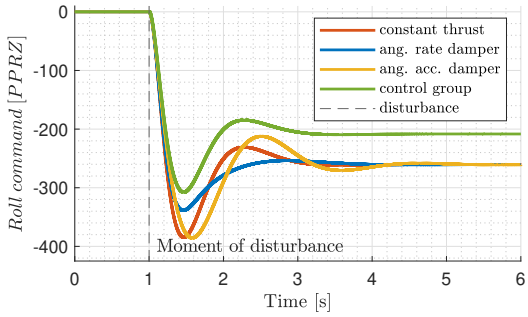

(b) Roll input command for disturbance rejection

Fig. 10: Step input for unintended behavior in the Hover phase.

rate damper strategy shows the lowest input command. The angular rate damper strategy also requires the least total input command for the manoeuvre. For the roll angles response, it can be seen that the angular rate damper has a higher settling time and overshoot than the control group, and the angular acceleration damper has even worse values. Nevertheless, all strategies show a stable step response.

For the disturbance tests, the maximum roll angle error, ϕ_{err}^{max}, can be compared. Looking at Figure 10a, we see that again the control group has a similar angle response compared to constant thrust. However, in Figure 10b a difference in input command exists between the control group and constant thrust strategy. The lowest ϕ_{err}^{max} can be seen with the angular rate damper strategy. The maximum command is lowest for the control group, followed by the angular rate damper strategy. The angular acceleration damper strategy has both a higher ϕ_{err}^{max} and a higher maximum command than the constant thrust strategy. Interestingly the total required amount of input command is equal for the investigated strategies except the control group.

Figure 11 shows a Nichols plot derived for the different control strategies. This plot is created for the entire joint structure controller, as displayed in Figure 8. The goal is to have the system's frequency response be as far from the critical point, the red cross, in the middle. The vertical distance from the system's frequency response to the critical point illustrates the gain margin, and the horizontal distance defines the phase margin. The phase and gain margin signify how many inaccuracies can exist within the controller without creating closed-loop instability. Here, the angular acceleration damper strategy seems the least stable, closely followed by the constant thrust strategy. The control group overlaps again with the constant thrust strategy. The angular rate damper is the most stable, having the biggest phase and gain margins of all the strategies.

TABLE IV: simulation results for the different strategies for disturbance rejection. For the maximum input command, the relative change is given with respect to the base reference of the control group. Based on simulations, the angular rate damper strategy is expected to perform the best by significantly improving disturbance rejection.

	Max. ϕ_{error}	**Max. input command**	**Relative change**	**Energy required for t=[0-5]**
control group	6.64 [deg]	307 [PPRZ]	100 [%]	1042 [PPRZ· s]
ang. rate damper	5.92 [deg]	339 [PPRZ]	110 [%]	1303 [PPRZ· s]
constant thrust	6.64 [deg]	384 [PPRZ]	125 [%]	1303 [PPRZ· s]
ang. acc. damper	6.72 [deg]	385 [PPRZ]	125 [%]	1303 [PPRZ· s]

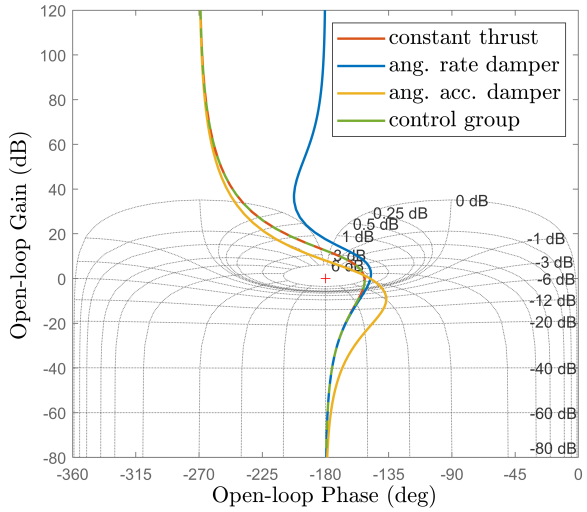

Fig. 11: Nichols plot for three strategies. Constant thrust and the control group overlap. The angular rate damper strategy should provide the best stability.

VII. Practical Verification

This section is focused on the joint structure's release mechanism and the test sequence.

A. Release Mechanism

The joint structure was built as per description mentioned in Section II. The separation was first tested as shown in Figure 12.

Figure 12 shows that the biplane is fixed to the ground. The thrust of the rotor is pointing straight up, meaning $\theta = 0\,[deg]$. The sequence of release is shown in Figure 13.

The fact that the quadrotor has no attitude control while being released is important for two reasons. First of all, the quadrotor releases best if the thrust vector is parallel to the thrust vector of the biplane. The motor mount of the quadrotor has to slide off a carbon plate, as shown in Figure 5, and if the thrust vectors are not aligned, this causes friction. This friction is enough to delay release on any of the four motor mounts. This delay can cause an even greater misalignment, resulting in more friction. Secondly, it is given that the aircraft do not communicate with each other. If the quadrotor was using attitude control, or even one of the damper strategies,

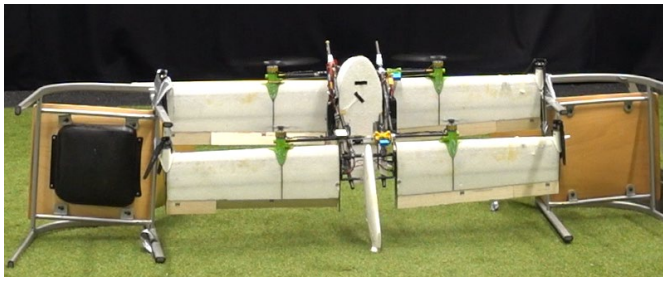

(a) Throttling up quadrotor to 70 %

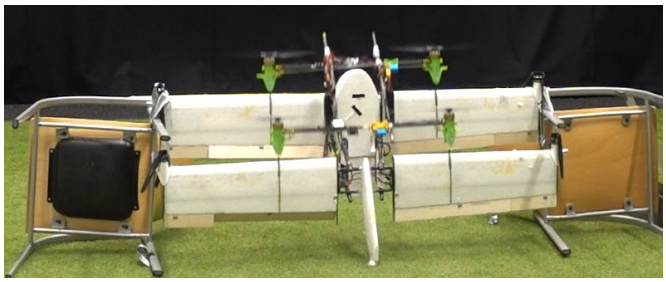

(b) Release mechanism engaged, quadrotor no attitude control

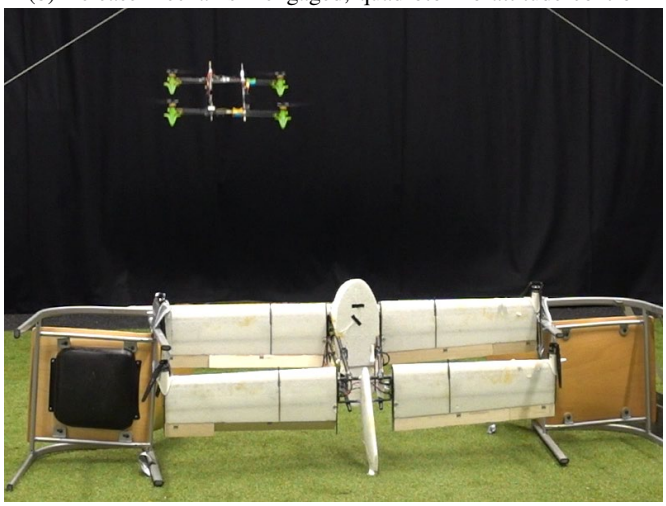

(c) Separate flight of quadrotor in hover

Fig. 12: Indoor release test of the quadrotor with the biplane in a static position

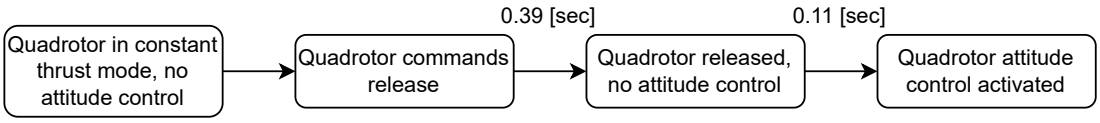

Fig. 13: Flowchart of the release mechanism

it could steer against the biplane, also misaligning the thrust vectors. No communication is also the reason why release is commanded from the quadrotor. The quadrotor has to know when it is released in order to timely activate its attitude control.

Experimental tests were performed, increasing the delay time between the signal of release and the initialisation of the attitude controller up to $1\ [sec]$. A side effect of this release method is that, in order to release successfully, the quadrotor will have no attitude control for a short time while disassembled from the biplane. On average, the quadrotor was clear of the biplane within $0.39\ [sec]$. The final delay time was iteratively set to $0.5\ [sec]$. This left enough time for the quadrotor to be clear of the biplane and not be in free flight for too long without active attitude control. The set-up was also tested with varying forward pitch angles up to $\theta = -18\,[deg]$. At 70% thrust, the quadrotor consistently released well with a control delay time of $0.5\ [sec]$. The quadrotor, during these tests, flew with a PID attitude control loop as opposed to the later implemented INDI.

The release system was also tested outdoors. The biplane was controlled by a separate pilot using an RC controller. At the moment of release, the goal was to have all the angles be as close to as possible to $[\phi, \theta, \psi] = [0, 0, 0]$. The little wind that was present meant that the joint structure would be slowly drifting, but this way, the thrust force of the quadrotor would be as parallel as possible to the biplane's thrust vector. The outdoor release tests outside were also successful. Figure 14 shows the three phases of the in-flight release.

Next, both platforms were proven to be capable of separate flight. In the case of the biplane, hover flight was carried out with the four outer rotor actuators. The control surfaces also aided in flight. The biplane was tuned for flight with the quadrotor attached. This means that, for the calculated control effectiveness, the inertia of the joint structure is taken into account, including the mass of the quadrotor. If the quadrotor releases, the actual control effectiveness increases due to the decreased inertia. Smeur et al. simulated that this would induce fast oscillations [27]. However, these fast oscillations were not found in the test flights of the biplane. One reason could be that the weight of the quadrotor sits close to the CG, which decreases the change in inertia.

B. Control strategies - test setup

The final test sequence consisted of the step input for both intentional and unintentional behaviour. The results of these tests could then directly be compared to the simulation results from section VI. The intentional step input was initialised via the RC controller. The step was set to $\phi = 18\ [deg]$ in both positive and negative roll angles. The tests were performed indoors to avoid any influence of wind. All the tests were performed in one sitting. In all cases, the thrust level for the quadrotor was set to 70%. Table V shows the mean throttle levels for the biplane for the various configurations.

TABLE V: throttle levels for different configurations

Mean Throttle level	Biplane	Quadrotor
control group	62.13 [%]	-
ang. rate damper	53.90 [%]	70 [%]
constant thrust	53.90 [%]	70 [%]
ang. acc. damper	54.21 [%]	70 [%]
separate flight	72.33 [%]	40 [%]

In order to create a repeatable and consistent step disturbance the joint structure dropped a weight. Two identical weights of 672 [grams] each were put on the sides of the biplane, one weight on either side. This created a net zero moment on the roll axis, not changing the CG, in the beginning of the test. The same release system that was created for the in-air disassembly was utilised, but instead of opening pins in the motor mount, a rope was released to which the weight was tied. After the release of one weight, the CG was shifted towards the weight that was still attached. This resulted in a constant roll moment. This step disturbance is comparable to [27], but Smeur et al. added a weight to the aircraft. This step disturbance was also simulated in Section VI-A.

An effort was made to keep the flight controller software similar to the greatest possible extent. The actuator dynamics, the filtering, and the sensor fusion all took place in a similar fashion for the quadrotor as well as the biplane. The main differences were the measurements and the actual control law.

C. Control strategies - test results

Figure 15 illustrates the overall result of all the (disturbance) input tests. Figure 15a and 15c show the mean response and input command of 6 repetitions for the angular rate and angular acceleration damper strategies, 5 repetitions for the control group and 3 repetitions for the constant thrust strategy. Table VI and VII show relevant parameters of the step input and disturbance.

Comparing Figure 15 with Figure 9 and 10, we find that the required inputs command for intended as well as unintended behaviour show a similar shape over time. However, the required command for disturbance rejection during the practical flights proved much more significant than in simulation. Figure 15a indicates that the step input tests show a very similar response for all the strategies. Overshoot for all of

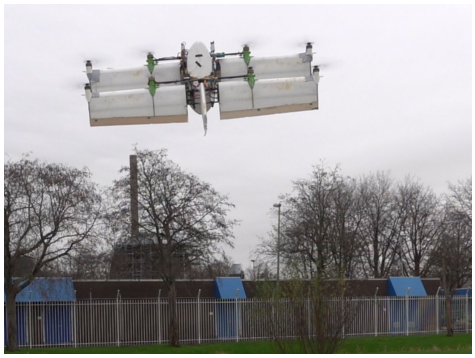

(a) Joint hover; Biplane in attitude INDI and quadrotor constant 70% thrust.

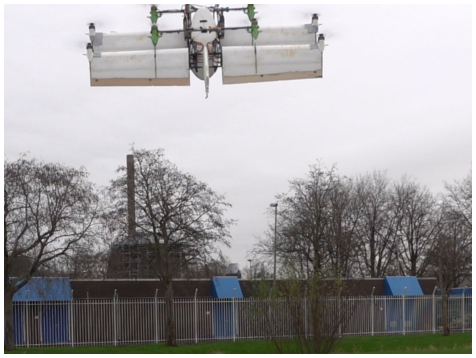

(b) Release mechanism engaged; The quadrotor has no attitude control.

(c) Separate flight; Both aircraft are in attitude control.

Fig. 14: Field release test - option 2.

TABLE VI: Practical results for the different strategies for intended step inputs.

	Settling time	**Max. input command**	**Energy required for t=[1-3.5]**
control group	0.89 [sec]	1018 [PPRZ]	360 [PPRZ· s]
ang. rate damper	0.84 [sec]	1024 [PPRZ]	368 [PPRZ· s]
constant thrust	0.84 [sec]	1060 [PPRZ]	403 [PPRZ· s]
ang. acc. damper	0.81 [sec]	1068 [PPRZ]	464 [PPRZ· s]

TABLE VII: Practical results for the different strategies for disturbance rejection. For the input command, the relative change is given with respect to the base reference of the control group.

	Max. ϕ_{error}	**Max. input command**	**Relative change**	**Energy required for t=[0-2.25]**
control group	5.19 [deg]	1199 [PPRZ]	100 [%]	1415 [PPRZ· s]
ang. rate damper	5.79 [deg]	1333 [PPRZ]	111 [%]	1745 [PPRZ· s]
constant thrust	6.29 [deg]	1425 [PPRZ]	119 [%]	1817 [PPRZ· s]
ang. acc. damper	6.92 [deg]	1523 [PPRZ]	127 [%]	1918 [PPRZ· s]

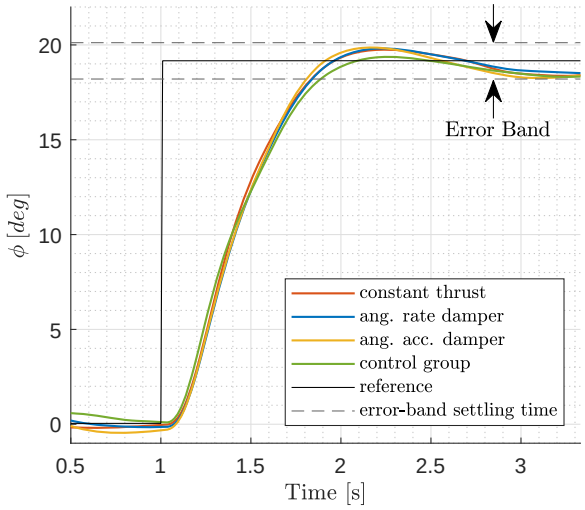

(a) Roll angle after intended Step input. Minimal change can be seen between the strategies for both overshoot and settling time.

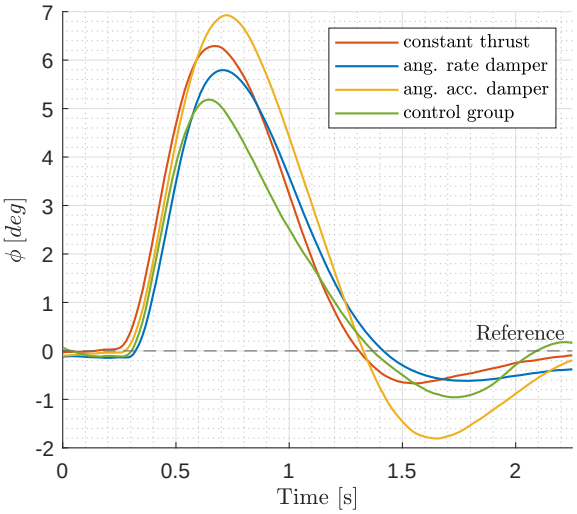

(b) Roll angle for disturbance rejection. The lowest ϕ_{err}^{max} is the goal. Angular rate damper strategy performed the best out of the three investigated strategies.

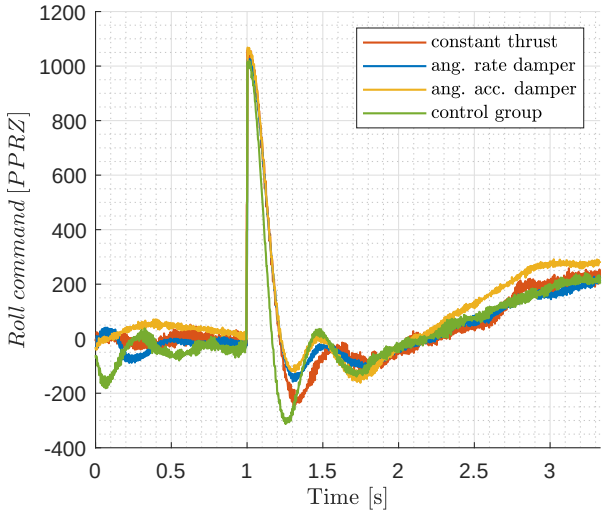

(c) Roll input command after intended Step input. After 2 [sec] the input gradually increases due to a head-up moment that needs to be counteracted.

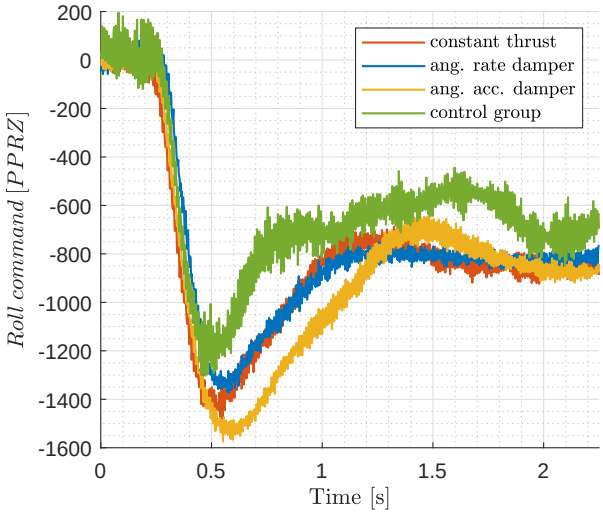

(d) Roll input command for disturbance rejection. The goal is to require the smallest CMD for disturbance rejection, so more CMD can be uses for intended behavior.

Fig. 15: Intended step input and step disturbance rejection in the Hover phase.

the strategies does not even cross the upper settling time error-band. The new steady-state roll angle was difficult to maintain for a longer time, due to a lack of space in the hangar. This also explains why the initial roll angle does not show a good steady-state value for some responses.

The required input command for the intended step input also shows a very similar response to simulations. The increase of the roll command after $t = 2\,[sec]$ can be explained by the fact that the joint structure needs to put in a constant roll offset to keep the roll angle at $\phi = 18\,[deg]$. This is referred to as a head-up moment, due to the flapping movement of the rotor [30].

Where the difference between strategies for intended behaviour is small, the difference for disturbance rejection is more significant. Table VII shows that the control group has the lowest ϕ_{err}^{max} and the smallest required input command, as expected. Comparing this base reference strategy to the other strategies, we find that the constant thrust would require 19% more peak input command to counteract the disturbance. The angular acceleration damper strategy performs even worse at 27% more required peak input command. As was the case in the simulations, the angular rate damper strategy performed the best, as it only required 11% more peak input command compared to the control group. The same order of performance

can be stated for ϕ_{err}^{max} and the total energy required.

At this point it should be borne in mind that the control group for this study acted as a base reference only, not as a feasible option. Of the options that were deemed feasible, the angular rate damper strategy proved to be the best.

VIII. Conclusion

This paper proposes an option of in-flight release of a conjoined quadrotor and biplane. How this was successfully developed is shown in Figure 14. In-flight release worked consistently and is tested up to a forward pitch angle of -18 [deg]. The study's second aim was to develop a joint control strategy with a focus on aiding the joint structure with disturbance rejection to as great an extent as possible. The biplane utilises a INDI controller. Given the fact that no intercommunication is available, the proposed control strategies for the quadrotor help with disturbance rejection, but they were also found to affect performance in terms of intended behaviour. Table VI shows that the impact of the different control strategies for intended step inputs is minimal. However, the gain with disturbance rejection is significant. Compared to the control group strategy, no active attitude control would result in 19% extra command. With the rate damper strategy active, this is reduced to 11% extra input command needed. Also, the maximum angle that the joint platform would reach due to the disturbance and the total amount of energy required is reduced with the active damper strategy. The angular acceleration damper strategy performed significantly worse for both the extra input command and the maximum angle.

IX. Discussion, further research

Future work could include examining how the quadrotor could be given more reference knowledge. This could be done with Geofencing to let the quadrotor know what phase of flight the joint structure is in. Another option would be to implement some form of communication. This way, an observer could be implemented in the quadrotor to better distinguish between planned manoeuvres and disturbances. Also, thrust could be reconsidered: it has been set at a constant value for the quadrotor, but this is not ideal in all phases of flight. Future work should also include the control strategies for the entire flight profile, including forward flight and transition.

References

[1] Voskuijl, M., Said, M., Pandher, J., Tooren, M. & Richards, B. In-flight deployment of morphing UAVs–a method to analyze dynamic stability, controllability and loads. *AIAA Aviation 2019 Forum*. pp. 3126 (2019)

[2] Kleij, C. Close formation flight control-with applications in commercial aviation. (2012)

[3] Saldana, D., Gabrich, B., Li, G., Yim, M. & Kumar, V. Modquad: The flying modular structure that self-assembles in midair. *2018 IEEE International Conference On Robotics And Automation (ICRA)*. pp. 691-698 (2018)

[4] Oung, R. & D'Andrea, R. The distributed flight array: Design, implementation, and analysis of a modular vertical take-off and landing vehicle. *The International Journal Of Robotics Research*. **33**, 375-400 (2014)

[5] Bai, S., Tan, S. & Chirarattananon, P. SplitFlyer: a Modular Quadcoptor that Disassembles into Two Flying Robots. *2020 IEEE/RSJ International Conference On Intelligent Robots And Systems (IROS)*. pp. 1207-1214 (2020)

[6] Wilson, D., Göktogan, A. & Sukkarieh, S. Guidance and Navigation for UAV Airborne Docking.. *Robotics: Science And Systems*. **3** (2015)

[7] Gosiewski, Z. & Ambroziak, L. Formation Flight Control Scheme for Unmanned Aerial Vehicles. *Robot Motion And Control 2011*. pp. 331-340 (2012)

[8] Xue, R. & Cai, G. Formation flight control of multi-UAV system with communication constraints. *Journal Of Aerospace Technology And Management*. **8**, 203-210 (2016)

[9] Quan, L., Yin, L., Xu, C. & Gao, F. Distributed Swarm Trajectory Optimization for Formation Flight in Dense Environments. *ArXiv Preprint ArXiv:2109.07682*. (2021)

[10] Ren, W. Consensus strategies for cooperative control of vehicle formations. *IET Control Theory Applications*. **1**, 505-512 (2007)

[11] Seo, J., Ahn, C. & Kim, Y. Controller design for UAV formation flight using consensus based decentralized approach. *AIAA Infotech@ Aerospace Conference And AIAA Unmanned... Unlimited Conference*. pp. 1826 (2009)

[12] Dehghani, M. & Menhaj, M. Communication free leader-follower formation control of unmanned aircraft systems. *Robotics And Autonomous Systems*. **80** pp. 69-75 (2016)

[13] Chao, Z., Zhou, S., Ming, L. & Zhang, W. UAV formation flight based on nonlinear model predictive control. *Mathematical Problems In Engineering*. **2012** (2012)

[14] Mahmood, A. & Kim, Y. Decentralized formation flight control of quadcopters using robust feedback linearization. *Journal Of The Franklin Institute*. **354**, 852-871 (2017)

[15] Turpin, M., Michael, N. & Kumar, V. Trajectory design and control for aggressive formation flight with quadrotors. *Autonomous Robots*. **33**, 143-156 (2012)

[16] Saldana, D., Gupta, P. & Kumar, V. Design and control of aerial modules for inflight self-disassembly. *IEEE Robotics And Automation Letters*. **4**, 3410-3417 (2019)

[17] Salih, A., Moghavvemi, M., Mohamed, H. & Gaeid, K. Modelling and PID controller design for a quadrotor unmanned air vehicle. *2010 IEEE International Conference On Automation, Quality And Testing, Robotics (AQTR)*. **1** pp. 1-5 (2010)

[18] Mo, H. & Farid, G. Nonlinear and adaptive intelligent control techniques for quadrotor uav–a survey. *Asian Journal Of Control*. **21**, 989-1008 (2019)

[19] De Wagter, C., Remes, B., Smeur, E., Tienen, F., Ruijsink, R., Hecke, K. & Horst, E. The NederDrone: A hybrid lift, hybrid energy hydrogen UAV. *International Journal Of Hydrogen Energy*. **46**, 16003-16018 (2021)

[20] Zhang, H., Song, B., Wang, H. & Xuan, J. A method for evaluating the wind disturbance rejection capability of a hybrid UAV in the quadrotor mode. *International Journal Of Micro Air Vehicles*. **11** pp. 1756829319869647 (2019)

[21] Smeur, E., Croon, G. & Chu, Q. Cascaded incremental nonlinear dynamic inversion for MAV disturbance rejection. *Control Engineering Practice*. **73** pp. 79-90 (2018)

[22] Smeur, E., Chu, Q. & Croon, G. Adaptive incremental nonlinear dynamic inversion for attitude control of micro air vehicles. *Journal Of Guidance, Control, And Dynamics*. **39**, 450-461 (2016)

[23] Mahony, R., Kumar, V. & Corke, P. Multirotor aerial vehicles: Modeling, estimation, and control of quadrotor. *IEEE Robotics And Automation Magazine*. **19**, 20-32 (2012)

[24] Theys, B., Notteboom, C., Hochstenbach, M. & De Schutter, J. Design and control of an unmanned aerial vehicle for autonomous parcel delivery with transition from vertical take-off to forward flight. *International Journal Of Micro Air Vehicles*. **7**, 395-405 (2015)

[25] Bellman, D. & Matranga, G. Design and Operational Characteristics of a Lunar-Landing Research Vehicle. (1965)

[26] Benallegue, A., Mokhtari, A. & Fridman, L. High-order sliding-mode observer for a quadrotor UAV. *International Journal Of Robust And Nonlinear Control: IFAC-Affiliated Journal*. **18**, 427-440 (2008)

[27] Smeur, E. Incremental Control of Hybrid Micro Air Vehicles. (Delft University of Technology,2018)

[28] Hattenberger, G., Bronz, M. & Gorraz, M. Using the paparazzi UAV system for scientific research. (Citeseer,2014)

[29] Tay, T., Mareels, I. & Moore, J. High performance control. (Springer Science Business Media,1998)

[30] Otsuka, H., Sasaki, D. & Nagatani, K. Reduction of the head-up pitching moment of small quad-rotor unmanned aerial vehicles in uniform flow. *International Journal Of Micro Air Vehicles*. **10**, 85-105 (2018)

II

Literature Review

2

Aircraft Classification

Before all of the different controllers and other subjects are discussed, it is important to distinguish the different physical types of aircraft. As mentioned in the introduction any type of aircraft that is flown unmanned, either remote-controlled or autonomous, is by definition a UAV. The next section will go over a range of different platforms classified into two main categories, rotorcraft and fixed-wing. Next platforms are explained that combine both the capability of the rotorcraft and the fixed-wing. These are referred to as hybrid aircraft.

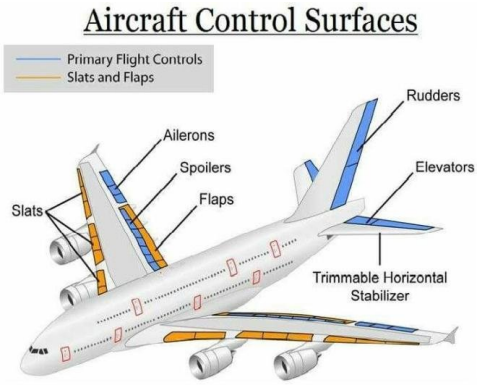

Figure 2.1: Overview of control of a typical fixed-wing aircraft [1].

The first main category of aircraft is the fixed-wing aircraft. This type of aircraft is known for its efficiency and endurance. An example is the typical dream liner aircraft manufactured in large by companies like Boeing and Airbus. fixed-wing aircraft make use of lift generated by their stationary wings. To create enough of a lift force to overcome gravity, they always require a certain horizontal speed. This means that the aircraft require some sort of runway for take off and landing. The most common fixed-wing aircraft consist of a fuselage, wings, and a horizontal and vertical stabiliser in the back. Control of this type of aircraft is mostly performed through control surfaces, see Figure 2.1. For the conventional fixed-wing airplane, control surfaces on the wings are responsible for roll manoeuvres (ailerons). The control surfaces on the horizontal stabiliser are responsible for pitch manoeuvres (elevators), and a vertical stabiliser is used for yaw manoeuvres (rudders).

The second category of aircraft is the rotorcraft. This type of aircraft has the benefit that it can hover and maintain its altitude without the need for horizontal speed. This means that a rotorcraft does not require a runway for landing and taking off. In the literature, rotorcraft are also referred to as a VTOL, **V**ertical **T**ake-**O**ff and **L**anding, aircraft. The best-known rotorcraft aircraft is the helicopter. A helicopter has a main rotor and a tail rotor; the latter is required to cancel the reaction torque generated by the main rotor. The main rotor can cause a pitch and/or roll moment on the aircraft through influencing the

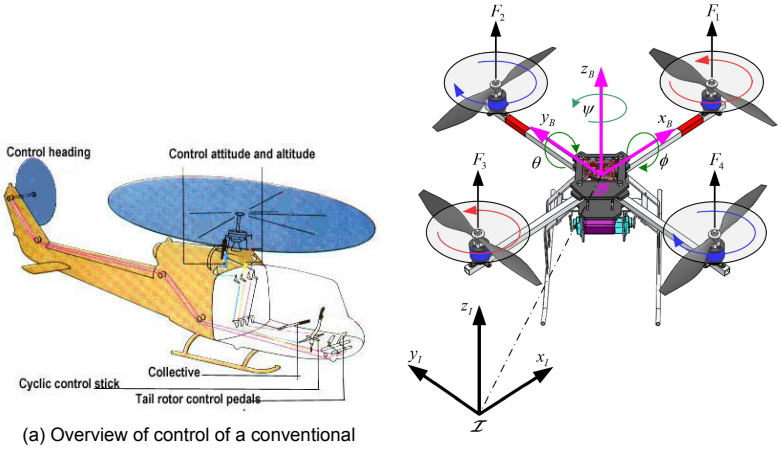

(a) Overview of control of a conventional helicopter [13].

(b) Overview of control of a Quadrotor [14].

Figure 2.2: Examples of rotorcraft aircraft

pitch of the main rotor at certain points of the cycle. This is achieved by means of a swashplate. See Figure 2.2a for an overview.

There is one particular type of rotorcraft that has become increasingly popular over the past few years: the multirotor, or the quadrotor to be more precise [15]. The quadrotor does not have the same mechanical complexity as a conventional helicopter, but it is still able to hover. Instead of using movable control surfaces like those in a fixed-wing aircraft or a rotor with a controllable pitch of the rotor blade, a multirotor uses differential thrust to control its attitude. To illustrate: a quadrotor has two of its propellers spin clockwise and the other two spin counter clockwise. This means that in the case of a desired roll or pitch moment, one clockwise and one counter clockwise rotating rotor will provide an equal amount of added thrust while the other two decrease that same amount of thrust. Thus, the net reaction torque is zero, but a moment is created around either the roll or the pitch axis. If the quadrotor wants to induce a yaw moment, the two (counter) clockwise rotors would spin up and the two others would spin down. This combination of differential thrust uses the reaction torque while not creating a moment in the pitch and/or roll axis. Figure 2.2b shows an overview of the control of a quadrotor.

A quadrotor's smart way of choosing which combination of actuators to increase or decrease in order to manoeuvre around one rotational axis is called control allocation. The use of control allocation deals with the fact that most rotorcraft are coupled aircraft. This means that spinning up a propeller not only causes a moment around one rotational axis but also creates a reaction torque, causing a moment around another axis. This means that a rotation around one axis is coupled with rotation around another axis. Control allocation enables the aircraft to control the aircraft in a decoupled manner, greatly simplifying the process.

In sum, a quadrotor's mechanical simplicity and the relative ease of decoupled control have made it a versatile platform with a wide application. Examples include platforms built for lifting heavy goods or for racing purposes. Other examples of multirotors include monocopters and gyroplanes, which can be used for military reconnaissance or recreational purposes [16, 17].

The third category, Hybrid aircraft, combines the two categories of aircraft just mentioned above. In general terms this means that a hybrid aircraft has both fixed-wings and has VTOL capability. Many forms of hybrid aircraft exist and in this section a few relevant examples will be explained. An extensive list of different hybrid aircraft can be found in a survey performed by Saeed et al. [21].

The first example of a hybrid aircraft is the quadplane [22]. Visually this looks the most like a hybrid aircraft, where the quadplane is just a quadrotor merged with a conventional shaped fixed-wing aircraft. For the hover phase the four propellers of the quadplane are responsible for lift and attitude control. In forward flight a pusher propeller provides thrust and control surfaces of the wings are actuated for attitude control. Figure 2.3a displays such a quadplane.

Another form of hybrid aircraft are tilt-wings [23]. As the name suggests the aircraft can have a tilt-able wing. In this case the wings would be vertical in hover and move to a horizontal position in forward flight. Compared to the quadplane, the benefit would be that the same actuator can provide

(a) Quadplane: SLT [18].

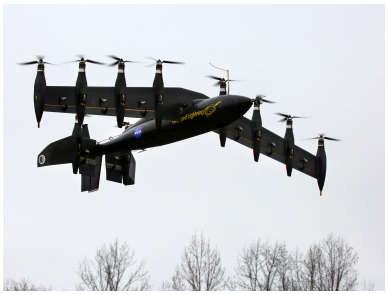

(b) Tilt-wing: NASA GL-10 [19].

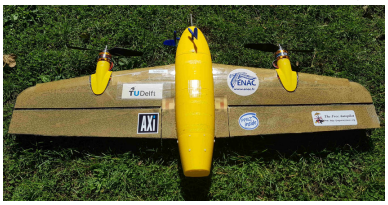

(c) Tailsitter: Cyclone [20].

Figure 2.3: Examples of various Hybrid aircraft.

thrust in both a vertical and a horizontal position. Figure 2.3b shows the NASA GL-10, one example of a tilt-wing aircraft.

In the case of a tailsitter, the aircraft will pitch its complete body to be able to fly in both hover and forward flight [24]. An example is the cyclone UAV, as shown in 2.3c [20]. The benefit of tailsitter is that no tilting mechanism or extra actuators are required for the aircraft to fly both in hover and forward flight. These tailsitters show a lot of potential, especially in robustness. The lack of these tilting mechanisms or extra actuators saves weight and reduces complexity. A clear example of these advantages is the Nederdrone.

Nederdrone

Figure 2.4: take off procedure of the Nederdrone [2].

For the Royal Netherlands Navy, the TU Delft has been developing a tailsitter aircraft that will be able to fly using a hydrogen fuel tank and a fuel cell combined with batteries [2]. This tailsitter is equipped with 12 motors and has two full wings, and this means that each of the four wing sections is equipped with three motors. The reason for this design was to create a robust and multi-redundant aircraft. The goal of the Nederdrone is to take off from and land on a helicopter deck of a ship and be able to fly for over 3 hours in forward flight. The purpose of the Nederdrone is to perform surveillance on the horizon. The Nederdrone and especially other tailsitters are known for having difficulty dealing with external disturbances in hover. Especially wind (gusts) can make controlling a tailsitter difficult. One of the reasons is their large aerodynamic surface being orthogonal to the wind direction in the hover phase [25]. Furthermore, the wings can be in a stalled condition due to their higher angles of attack during either transition or hover.

In order to deal with these challenges, many different control theories have been developed. The next section will go over a few of the relevant ones for this research.

3

Control-loop Strategies

3.1. General Control theory

As mentioned in the previous chapter multirotors have seen a rise in popularity and in particular the quadrotor. One of the reasons is the mechanical simplicity while still having a very agile platform capable of very precise attitude/position control. Most multirotors are inherently unstable and require constant active control from a flight computer to keep it stable [26]. This control can be illustrated in a general loop as can be seen below in Figure 3.1.

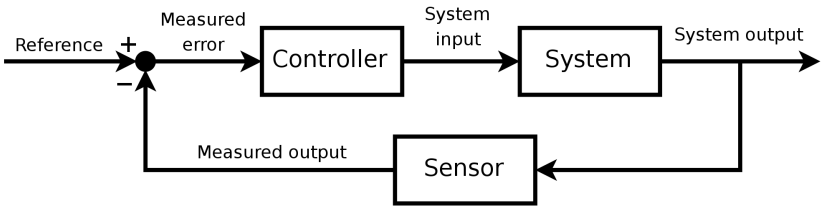

Figure 3.1: A simplified control loop [3].

The ”Reference” is the input from the pilot, a ground station or a desired state autonomously determined by the onboard computer. This ”Reference” will be compared to the ”Measured output” acquired with onboard sensors, resulting in a ”Measured error”. A ”Controller” will generate an input that will be put into the system. This ”System input” can be a deflection on a control surface or a set-point on an actuator. Actuators can be propellers, but also jets or electronic ducted fans. The ”System” block resembles how the aircraft behaves on the input. These dynamics depend on the aircraft's physical properties and are very hard to model, primarily due to the dynamic nonlinearities of the system. Section 3.6.2 will explain more in-depth why particular aircraft, like the multirotor, are nonlinear systems.

Sensors measurements are not perfect. They often are contaminated with noise and/or have a bias. This means that the system would either require filtering or sensor fusion in order to get an adequate measured output. The challenges of the system and the sensors require the controller to be robust and compensate for these uncertainties in the control loop. The following sections will explain some of the most popular and relevant control theories, all proposing solutions to the controller portion of the control loop.

3.2. PID

The most popular controller type has been proportional-integral-derivative, PID, control. PID control is a linear controller. If a PID controller is used with a nonlinear system, it yields approximation errors. However, PID is a robust controller, and therefore most of the nonlinear systems can still be controlled but not optimal due to these approximation errors. Yet in most cases, it is sufficient. Figure 3.2 shows the general form of PID control.

Compared to Figure 3.1 the controller block now consists of three parts; The **P**roportional, the **I**ntegral and the **D**erivative. Note that the working principle of PID revolves around a feedback loop.

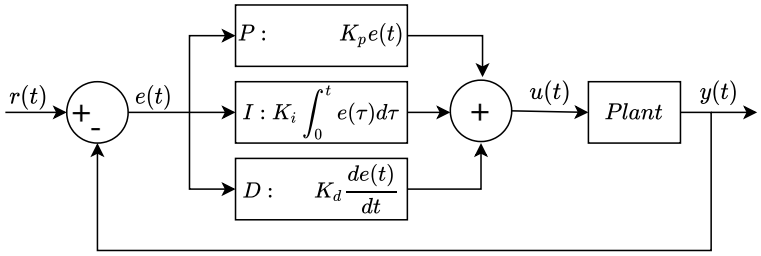

Figure 3.2: PID Schematics

The goal for the PID controller is to get $e(t) \to 0$. The Proportional gain has a linear relation between the measured error and the gain. Controllers just using the Proportional gain exist, but these systems usually undergo an overshoot and oscillate around the desired new situation. The Derivative gain is proportional to the rate of change of the error, which dampens out the oscillation. However, an offset between the new state and the desired new state can still occur since both the Derivative and Proportional gains become very small when the signal reaches the new state. The Integral gain integrates the error over time. Every time step an error is present, the I gain will increase every time step. This deals with the steady state error, but the I gain can also create problems. Situations can occur where the controller detects an error in its states, but the system cannot deal with this physically. Imagine a rotorcraft, but the propellers are not attached, and the motors can still spin freely. The aircraft is tuned with the propellers on, but no thrust is generated if the propellers are absent. If the aircraft detects a slight offset, the P and D gain will stay relatively low since the absolute error is marginal. However, The I gain will increase every time step until the maximum command is given. If the controller is not reset and the propellers are mounted on the motor, the gain will be very high from the start, causing instability to the aircraft. This occurrence is also referred to as Integral Windup [27].

PID overall has proven to work very well for quadrotor UAV's where the aerodynamic properties of the platform do not change too much, but for some VTOL platforms, PID seems to have a more difficult time controlling the platform well. For example, a tailsitter has a large vertical cross-section when in hover, being the wing. This large vertical cross-section is very prone to wind and therefore fast reactions on the caused accelerations is required. Also, during transition from hover to forward flight the VTOL platform undergoes different aerodynamic effects, and the PID controller has to compensate for this with the integrator. However, this is only accomplished slowly [2].

3.3. NDI

To deal with the approximation issues that come with PID controllers for nonlinear systems, nonlinear control is researched. One of these control methods is Nonlinear Dynamic Inversion [28–30].

First a model of an aircraft can be written in state space form. The general state space form is defined as:

$$\dot{x} = f(x) + g(x)u \tag{3.1}$$

In companion form this state space model is written as:

$$\begin{bmatrix} \dot{x}_1 \\ \vdots \\ \dot{x}_{n-1} \\ \dot{x}_n \end{bmatrix} = \begin{bmatrix} x_2 \\ \vdots \\ x_n \\ b(x) \end{bmatrix} + \begin{bmatrix} 0 \\ \vdots \\ 0 \\ a(x) \end{bmatrix} u. \tag{3.2}$$

3.2 implies that any nonlinear terms in the state space notation now only influence x_n, as well as the input. Furthermore a virtual input is introduced. This is defined as:

$$v = b(x) + a(x)u \quad \Leftrightarrow \quad u = a^{-1}(x)(v - b(x)) \tag{3.3}$$

Not all nonlinear systems can be easily written in a companion form. In those cases, it can still be achieved by performing an Input-Output Linearization. With Input-Output Linearization, the output function, y here, is differentiated until the input, u, is directly part of the equation. Then a and b can be

derived such that Equation 3.3 is valid. The amount of times the output function needs to be differentiated is called the system's relative degree, r. If r is smaller than the order of the system determined by the states, then part of the system becomes unobservable. In that case, it is difficult to determine if the system is stable so that the controller can work properly. In the end, Input-Output Linearization transitions the system to be controlled in a linear manner.

If a companion form is defined, the introduced virtual input, v, still needs to be derived. This is system-dependent, meaning that the v is defined differently for every other aircraft. Figure 3.3 shows the control-loop visualisation of NDI. Here again it becomes clear that the controller requires information from both the $f(x)$ and $g(x)$ matrices. That means that the NDI controller relies on complete knowledge of the dynamics of the system. However, we are not dealing with perfect conditions. The inertia of the platform changes constantly, disturbances are perturbed on the platform, and even the estimation of the Input-Output relation is not fully known. In theory, this controller could work, but in practice, it would probably under or overestimate the platform's performance, creating approximation errors. Also, actuator constraints, such as saturation, are not considered in the system. An extension on NDI is explained in the next section, which is a more robust controller.

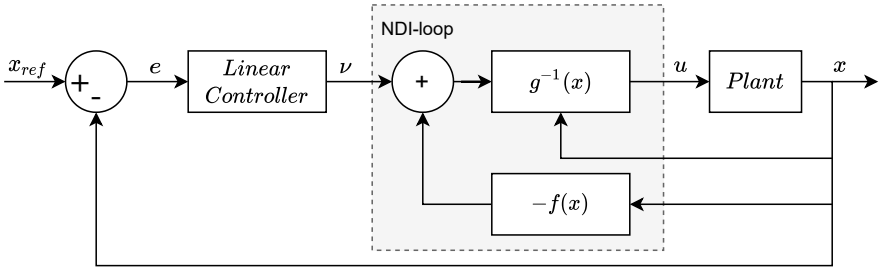

Figure 3.3: NDI inner loop and linear control outer loop

3.4. INDI

In order to deal with the limits from NDI Incremental Nonlinear Dynamic Inversion (INDI) has been researched [31, 32]. The benefit is that complete knowledge of the system dynamics is not required to be known. INDI uses measurements of the states of the aircraft in order to control the platform. Where NDI controls the required virtual input of the system, INDI controls a change in input. For example, an aircraft has ailerons to control the roll angle. In the case of NDI, the input calculated was a deflection angle. This angle relates to a particular rotational rate. INDI, however, constantly calculates a change in deflections, controlling the angular acceleration around the roll axis. This difference is vital since less of the system model dynamics is required to be known. Only the g-matrix from Equation 3.1 should be defined and not the $f(x)$ matrix anymore.

First, a system will be defined as a general function dependent on a state, x, and an input, u.

$$\dot{x} = f(x, u) \tag{3.4}$$

The two partial derivatives are then defined as:

$$\frac{\partial f(x,u)}{\partial x} = F(x_0, u_0) \quad and \quad \frac{\partial f(x,u)}{\partial u} = G(x_0, u_0) \tag{3.5}$$

Equation 3.4 can now be rewritten as:

$$\dot{x} \approx \dot{x}_0 + F(x_0, u_0)\Delta x + G(x_0, u_0)\Delta u \tag{3.6}$$

If time-scale separation is used on Equation3.6, this yields:

$$F(x_0, u_0)\Delta x \ll G(x_0, u_0)\Delta u \tag{3.7}$$

$F(x_0, u_0)\Delta x$ can then be taken out of the equation. Now equation 3.8 will become:

$$\dot{x} \approx \dot{x}_0 + G(x_0, u_0)\Delta u \tag{3.8}$$

If we add in a virtual controller, v, our main INDI equation will then become:

$$\Delta u \approx G^{-1}(x_0, u_0)(v - \dot{x}_0) \tag{3.9}$$

Equation 3.9 shows that the knowledge of $F(x_0, u_0)$ is no longer required. However, $G(x_0, u_0)$ and the virtual input v must be known. $G(x_0, u_0)$ is also referred to as the control effectiveness matrix and can either be theoretically derived for a particular type of aircraft, see Section 3.5, or can be derived from practical flight data.

The derivation of the virtual input comes from the inertial measurement unit, IMU, and depends on the aircraft type. The following section will derive an example of the definition of v in the case of Multirotors.

INDI has performed well on platforms like tailsitters, including the Nederdrone [2, 33, 34]. The reason is that the flight envelope of these aircraft cover vastly different dynamics in the different flight phases, and INDI has proven to be a more robust control technique compared to PID, for example. Furthermore, INDI deals better with disturbances. As mentioned before, disturbances are challenging to deal with in the hover phase of hybrid UAVs.

3.5. INDI Applied to Multirotors

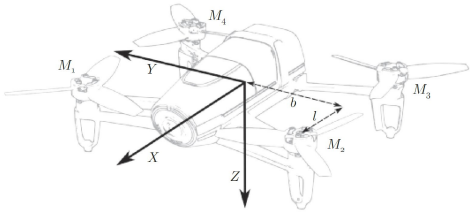

Figure 3.4: schematics of a multirotor, quadrotor in this case, for axes definition [4]

In this section, the INDI control technique will be applied to Multirotors. It will closely follow the PhD work of E.J.J.Smeur [4]. As mentioned in Section 2, multirotors have multiple actuators. The actuators can create a certain moment around the platform's centre of gravity. In the case of both the multirotor and the VTOL, we define three rotational axes where the following law holds:

$$M = I_v\dot{\Omega} + \Omega \times I_v\Omega = M_a(\Omega, v) + M_c(\omega) + M_r(\omega, \dot{\omega}, \Omega) \tag{3.10}$$

, where M is the total moment, I_v is the inertia around the rotational axis, ω is the angular rate around the body z-axis and $\dot{\omega}$ is the angular acceleration around the body z-axis. M_a is the moment due to aerodynamics, M_c is the moment due to the controls, M_r is the moment due to the gyroscopic effect of the rotors and Ω is the angular rotation vector. Equation 3.10 provides a starting point of a dynamics model of a multirotor. this equation can be rewritten as solution for the angular acceleration:

$$\dot{\Omega} = I_v^{-1}(M_a(\Omega, v) - \Omega \times I_v\Omega) + I_v^{-1}(M_c - M_r) \tag{3.11}$$

This can be also written as:

$$\dot{\Omega} = F(\Omega, v) + \frac{1}{2}G_{1_q}\omega^2 + T_s G_2\dot{\omega} - C(\Omega)G_3\omega \tag{3.12}$$

here $F(\Omega, v) = I_v^{-1}(M_a(\Omega, v) - \Omega \times I_v\Omega)$. Note that all these terms do not depend on the behaviour of the actuators. G_{1_q}, G_2, G_3 and $C(\Omega)$ are defined as:

$$G_{1_q} = 2I_v^{-1}\begin{bmatrix} -bk_1 & bk_1 & bk_1 & -bk_1 \\ lk_1 & lk_1 & -lk_1 & -lk_1 \\ k_2 & -k_2 & k_2 & -k_2 \end{bmatrix} \tag{3.13}$$

$$G_2 = I_v^{-1}T_s^{-1}\begin{bmatrix} 0 & 0 & 0 & 0 \\ 0 & 0 & 0 & 0 \\ I_{r_{zz}} & -I_{r_{zz}} & I_{r_{zz}} & -I_{r_{zz}} \end{bmatrix} \tag{3.14}$$

$$G_3 = I_v^{-1}\begin{bmatrix} I_{r_{zz}} & -I_{r_{zz}} & I_{r_{zz}} & -I_{r_{zz}} \\ -I_{r_{zz}} & I_{r_{zz}} & -I_{r_{zz}} & I_{r_{zz}} \\ 0 & 0 & 0 & 0 \end{bmatrix} \tag{3.15}$$

$$C(\Omega) = \begin{bmatrix} \Omega_y & 0 & 0 \\ 0 & \Omega_x & 0 \\ 0 & 0 & 0 \end{bmatrix} \tag{3.16}$$

, where I_v is the inertia matrix of the aircraft, b is the width of the aircraft, k_1 is the force constant of the rotors, l is the length of the vehicle and k_2 is the moment constant of the rotors. See Figure 3.4 for the visual definition of the width and length of the vehicle.

Applying the taylor expansion on equation 3.12, neglecting higher order terms, gives:

$$\begin{aligned} \dot{\Omega} = {} & F(\Omega_0, v_0) + \frac{1}{2}G_{1_q}\omega_0^2 + T_s G_2 \dot{\omega}_0 - C(\Omega_0)G_3\omega_0 \\ & + \frac{\partial}{\partial \Omega}(F(\Omega, v_0) + C(\Omega)G_3\omega_0)|_{\Omega=\Omega_0}(\Omega - \Omega_0) \\ & + \frac{\partial}{\partial v}(F(\Omega_0, v))|_{v=v_0}(v - v_0) \\ & + \frac{\partial}{\partial \omega}(\frac{1}{2}G_{1_q}\omega^2 - C(\Omega_0)G_3\omega)|_{\omega=\omega_0}(\omega - \omega_0) \\ & + \frac{\partial}{\partial \dot{\omega}}(T_s G_2 \dot{\omega})|_{\dot{\omega}=\dot{\omega}_0}(\dot{\omega} - \dot{\omega}_0) \end{aligned} \tag{3.17}$$

The first term, $F(\Omega_0, v_0) + \frac{1}{2}G_{1_q}\omega_0^2 + T_s G_2 \dot{\omega}_0 - C(\Omega_0)G_3\omega_0$, can be replaced by $\dot{\Omega}_0$ since this term implies the angular acceleration based on current inputs. The current angular acceleration can be obtained from the current angular rates, which can directly be measured from the IMU using three gyroscopes. Secondly, similar to Equation 3.6, time-scale separation can be used if the actuators create moments faster than the aerodynamic and the precession moments. This negates the second and third term. The new solution for $\dot{\Omega}$ then is:

$$\dot{\Omega} = \dot{\Omega}_0 + G_{1_q} diag(\omega_0)(\omega - \omega_0) + T_s G_2(\dot{\omega} - \dot{\omega}_0) - C(\Omega_0)G_3(\omega - \omega_0) \tag{3.18}$$

The measurements on multirotors are usually noisy. This means that a filter would need to be applied. all $\ldots_0$ terms will therefore be replaced with $\ldots_f$ terms, implying these are the filtered measurements. The application of the filter implies a time delay. The time delay is constant for all measurements and this cancels out any inequalities in the general equation and therefore all terms can be rewritten with the new subscript in the same manner.

The derivation of $\dot{\Omega}$ now becomes:

$$\dot{\Omega} = \dot{\Omega}_f + G_{1_q} diag(\omega_f)(\omega - \omega_f) + T_s G_2(\dot{\omega} - \dot{\omega}_f) - C(\Omega_f)G_3(\omega - \omega_f) \tag{3.19}$$

The $\dot{\omega}$ can be discrete approximated by $(\omega - \omega z^{-1})T_s^{-1}$, yielding:

$$\dot{\Omega} = \dot{\Omega}_f + G_{1_q} diag(\omega_f)(\omega - \omega_f) + G_2(\omega - \omega z^{-1} - \omega_f + \omega_f z^{-1}) - C(\Omega_f)G_3(\omega - \omega_f) \tag{3.20}$$

Next all the $(\omega - \omega_f)$ terms can be isolated:

$$\dot{\Omega} = \dot{\Omega}_f + (G_{1_q} diag(\omega_f) + G_2 - C(\Omega_f)G_3)(\omega - \omega_f) - G_2 z^{-1}(\omega - \omega_f) \tag{3.21}$$

The equation can now be inversed, yielding a solution for ω. Since ω is the input command for the motors, the $\ldots_c$ subscript is added.

$$\omega_c = \omega_f + (G_{1_q} diag(\omega_f) + G_2 - C(\Omega_f)G_3)^+(v - \dot{\Omega}_f + G_2 z^{-1}(\omega_c - \omega_f)) \tag{3.22}$$

, with $\ldots^+$ meaning the Moore-Penrose pseudoinverse of a matrix.

Note that v is the virtual input, defined as the reference angular acceleration. ω_c is the current motor command, and ω_f is the motor command of the previous iteration.

G_3 yields part of the gyroscopic effect of the rotors. If the term is left out of the equation, the effect is marginal for the input approximation. For example, for a typical dataset created by E.Smeur, the approximation error was 0.2%. G_2 describes the gyroscopic effect on yaw. This effect is more significant than G_3, so this term continues to be part of the equation. The term G_{1_q} mentioned in Equation 3.13 shows the relation between the rotational speed of the individual rotors and the moment generated. It should be noted that this relation is quadratic, see Section 3.6.2. This term must also stay in the equation. The final control law of INDI for multirotors is now defined as:

$$\omega_c = \omega_f + (G_1 + G_2)^+(v - \dot{\Omega}_f + G_2 z^{-1}(\omega_c - \omega_f)) \tag{3.23}$$

A control loop can be designed using the final control law. In Figure 3.5, the overall control structure is shown of INDI applied to MAV:

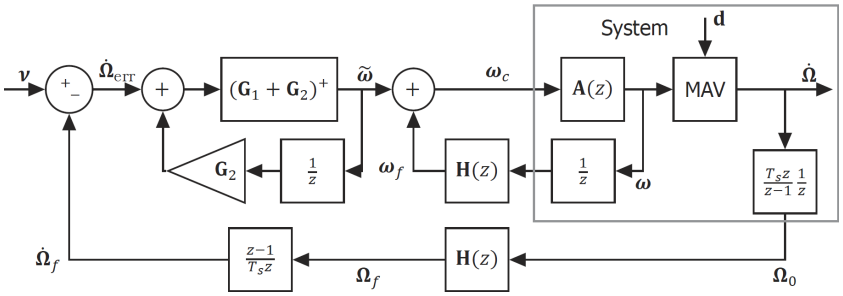

Figure 3.5: INDI Schematics, Smeur et al. [4].

Actuator Dynamics

ω_c is defined as the motor command input. The new command to the actuator is an input into the dynamic system. In the case of rotors, the propeller needs time to spin up or down to the new desired situation and cannot physically immediately follow the desired input. This behaviour can be described in terms of actuator dynamics and requires modelling. The actuators in multirotors consist of the propeller, the motor, the Electronic Speed Controller (ESC) and the battery. These parts influence the actuator dynamics; For example, a larger propeller would take longer to spin up than a smaller one. The actuator dynamics, just like the system dynamics, yields the relation between the input and output.

In Figure 3.6 this relation is visually shown. The data in this figure is derived by measuring the Revolutions per minute, RPM, as a response to different Pulse Width Modulated, PWM, input signals. The hardware used to derive this data is mentioned in Section II.A of the Scientific Report. The output amplitude does not perfectly match the input amplitude due to scaling. However, the output does not instantly follow the input. A first-order transfer function can model this relation. From literature, this proved to be accurate enough for most rotor actuators [35]. In Figure 3.5, the actuator dynamics is displayed with the **A(z)** block.

Cascaded controller

The multirotor can not be controlled entirely with the control loop mentioned in Figure 3.5. The input reference for the control loop is the virtual input, v, and is acquired using two additional control feedback loops. These outer loops control the angles and the angular rate of the multirotor. An overview of the outer loops with INDI as the inner loop is shown in Figure 3.7.

Attitude angles are defined as η. The attitude angles can be defined in different forms. The first form can be the Euler angles, usually defined in radians for roll, pitch and yaw. However, the attitude angles have to be derived from the angular rates, and the conversion from the rates to Euler angles are nonlinear and high-computational intensive calculations. For small angles however integration of the angular rates to obtain the attitude can still be sufficient. The other method is attitude feedback using purely the quaternion representation [36]. Quaternions are a complex notation for angles. The benefit is that no singularities exist, which is the case with Euler angles. These singularities are also referred to as Gimbal-lock. The reference in the quaternion representation would be defined as:

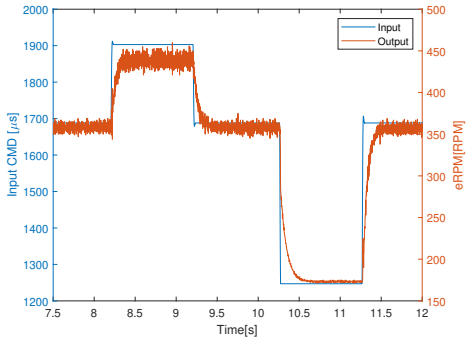

Figure 3.6: Actuator Dynamics - Input and Output over time

$$q_{err} = q_{ref} \otimes q_m^* \tag{3.24}$$

Here $\otimes$ is the Hamilton product, and $...^*$ is defined as the complex conjugate. q_{ref} is the desired attitude state, q_m is the measured attitude state and q_{err} is the difference between the two. From this Ω_{ref} is then defined as:

$$\Omega_{ref} = K_\eta [q_1^{err} q_2^{err} q_3^{err}]^T \tag{3.25}$$

The next step is to calculate the virtual control input, ν, which is defined as:

$$\nu = \dot{\Omega}_{ref} = K_\Omega [\Omega_1^{err} \Omega_2^{err} \Omega_3^{err}]^T \tag{3.26}$$

For the feedback loop the gains are multiplied by a defined proportional gain, K_η and K_Ω. These proportional gains are similar to the P and D gains of the PID controller, described in Section 3.2. The fact that a combination is used with PD-control for the outer loops and INDI for the inner loop is also referred to a Cascaded controller.

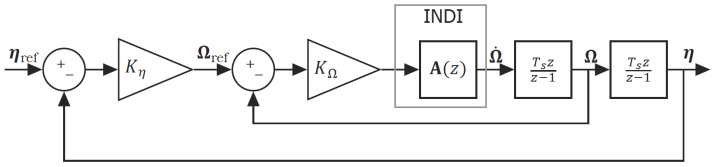

Figure 3.7: Schematics of an INDI innerloop and two outerloops with proportional control [4].

For attitude estimation the IMU is used. The IMU consists of three gyroscopes and three accelerometers. The three gyroscopes measure angular rate and the accelerometers measure lateral acceleration of the vehicle. These measurements are then used for feedback to the INDI controller and the linear controller.

Actuator saturation

The INDI controller will, in practice, send an input command to the actuator. In these calculations, the maximum physical output of an actuator is not taken into account. This means that if the desired input command exceeds the maximum command of an actuator, the value will just be limited to the maximum possible command due to the physical limitations. This is also called saturation of the actuator.

Actuator saturation in itself would not be a problem if a single actuator were responsible for a single control axis separately, implying complete decoupled control. From Section 2, however, it became clear that multirotors use a combination of actuators in order to create a moment around a quadrotor. In the case of a quadrotor, one actuator can influence all three rotational axes, which can cause problems.

If, for example, a high yaw rotation and a high roll rotation are desired simultaneously, one or more of the actuators can reach their limit. The controller does not take the saturated value into account; It will merely ask as much as possible from the actuator. This will result in an offset in the expected state

with respect to the actual state. The robust nature of INDI will deal with this, but one can understand that this can limit the aircraft's performance.

However, actuator saturation can have serious consequences. If one actuator saturates due to a very high yaw command, it has no control authority left to help control around another axis or provide more thrust. The INDI controller quickly wants to counteract the disturbance, especially with disturbance rejection scenarios. Since yaw control is gained by the reaction torque instead of a moment, this requires a lot of control authority from the different actuators. Equation 3.13 shows this; The third row resembles the control authority about the yaw axis. Compared to the other two axes, the moment arms from the C.G. to the actuators are missing, decreasing the control authority. For multirotors, the command to an actuator usually sums up the command for roll, pitch, yaw and thrust. If yaw control would relatively require more control authority than control about the other axis, this leaves less control authority for the other axes.

Another effect is that the overall thrust can be lowered due to actuator saturation. For example, a quadrotor requires 75% of the maximum available thrust to maintain a hover. If the aircraft momentarily requires a lot of yaw control authority in a disturbance rejection scenario, the controller might require a change of 30% thrust. For the propellers that would need to rotate slower, the new thrust level would be 45%. The propellers that need to rotate faster, would be set to 105%, but are limited to 100%. This lowers the average thrust level. The result can be that the aircraft will unintentionally fall out of the sky.

A solution to forever prevent actuator saturation using INDI has not been found. However, control allocation can be used to minimise actuator saturation or more eminently prioritise what axis is more important not to suffer from negative effects of saturation. In the case of a multirotor or a hybrid aircraft in hover, priority is usually given to roll and pitch over yaw and thrust. E.Smeur has proved that using a Weighted Least Squares algorithm can properly prioritise roll and pitch over yaw increasing the stability of a multirotor [37].

3.6. Control modes for UAVs

Apart from the type of controller, the type of reference signal is also crucial for the performance and capability of the platform. For most consumer UAVs, the controller reference is defined in the form of a flight mode determined by the autopilot software. The autopilot software, like Ardupilot or Paparazzi UAV, determines what type of reference the controller is steering towards [38, 39]. The most basic form of control is having direct authority over the different control surfaces or motors. With radio controlled airplanes this is comparable to directly wiring the servo's to an RC receiver and converting the stick input of the radio controller to a position on the servo. The autopilot software can realise this in software by not having any active control, basically mimicking this direct wiring option. Other flight modes usually involve a different control method. The reference can be a certain angle, height, or an translational or rotational rate in any of the 6 degrees of freedom (DoF). Depending on the different flight modes, different sensors need to be equipped on the UAV. Documentation for the PX4 has a good overview of the different control modes [40]. The following sections will cover two relevant control modes, attitude control and position control.

3.6.1. Attitude Control

The first control mode is called attitude control. The reference for the aircraft in this mode are usually the body reference angles, pitch(θ), roll(ϕ) and yaw(ψ). This means that the states that will be controlled are these same body reference angles or their derivatives, the angular rates. For INDI the derivatives of the angular rates, the angular accelerations, are also used for control.

Sections 3.2, 3.3 and 3.4 explained the attitude control for an UAV. For INDI, the overview shown in Figure 3.7 enclosed the attitude control for a multirotor. The combination of the linear PD controller for the angle and angular rates control loop and the INDI controller for angular accelerations is also referred to as a Cascaded Controller; a combination of two types of controllers.

3.6.2. Position Control

Where attitude control is tracking a zero-error for angles, fully autonomous or even semi-autonomous flights require more control loops. With attitude control, the pilot determines the height, velocity and position of the UAV usually with its eyes by means of line of sight. For fully autonomous or semi-autonomous control, the aircraft performs these calculations on-board.

Firstly a new set of sensors is required, for example, a GPS, a magnetometer or an altimeter. These sensors will then form the feedback of the outer loop of the total control system. This is because now parameters like horizontal and vertical position should be controlled. Figure 3.8 shows an cascaded INDI control architecture for position control and Figure 3.9 shows an position control architecture using only PID [4].

Position control for hybrid aircraft is approached differently by a PID compared to the INDI controller. Position control using PID for hybrid aircraft usually is achieved by implementing a modal controller. A modal controller means that the aircraft can be put in different flight modes where the controller has different PID gains due to different effects of the actuators in the different phases of flight. The attitude of the UAV indirectly controls the position. This can pose a challenge for hybrid aircraft since the aircraft is flying in different flight regimes. If hover and forward flight were the only two flight phases, this could be solved by having different gains for the two phases. However, a case exists where a hybrid flies in hover but has a forward speed to cancel out the wind. The modal controller does either know forward flight or hover, which makes the modal controller not ideal in the ”in-between-phases”.

E.Smeur solved this problem using a different method. Two INDI controllers are used, using the lateral accelerations, speed and position for the position control. The main parameter that changes is the control effectiveness depending on the different scenarios. For tailsitters, airspeed and pitch angles are used to schedule the control effectiveness of the different actuators. This makes using a model controller unnecessary since the aircraft can effectively be controlled in every situation across the flight envelope.

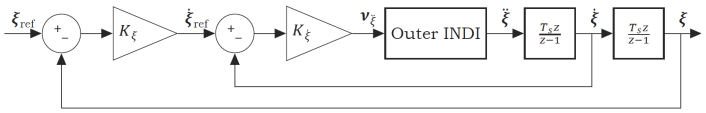

Figure 3.8: Schematics of an INDI innerloop and two outerloops with proportional control for position control [4].

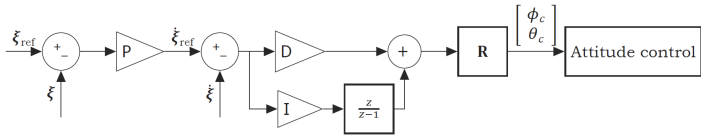

Figure 3.9: Schematics of an PID contoller for position control [4].

ξ_{ref} is defined as the reference position. These can either be derived from pre-planned waypoints and directly sent via a groundstation.

Nonlinearity of a system model

In Section 3.1 a difference has been mentioned between controlling a linear and nonlinear system. This section will explain the difference and why the multirotor is a nonlinear system.

A lot of control theory is based on a Linear system. A system is linear if the superposition principle holds. The superposition principle is two-fold. Firstly the additivity property is defined as follows:

$$H(x_1 + x_2) = H(x_1) + H(x_2) \tag{3.27}$$

And secondly, a linear system has to property of homogeneity, defined as follows:

$$H(ax) = aH(x) \tag{3.28}$$

, Where x_1 and x_2 are two input signals, a is any scalar value and H is defined as the system.

In order to determine whether or not a multirotor system is linear, all the different steps in the dynamics of the system can be individually considered. Namely, the total system will be nonlinear if one part is nonlinear. The calculated input that either PID or INDI calculates is a PWM input that will run into the ESC. This PWM signal will be converted into a certain rotational speed of a propeller. This is a linear relation. However, the RPM and the Thrust generated has a quadratic relation. Below the formula is given for the amount of Lift generated for a rotary-wing:

$$L = \frac{1}{2}\int_0^l \rho c V^2 C_L dl \tag{3.29}$$

,where l is the length of the propeller, ρ is defined as the air density, C_L is the dimensionless lift coefficient, c is the chord length and V is the local flow velocity. Here, the relation between V and the $Lift$ is quadratic. This is the first nonlinear part of the system. However, in practice if this is linearised this yields a marginal approximation error [4].

Next is the relation between the lift force of an actuator and the moment on the rigid aircraft body. This relation has previously been mentioned in Equation 3.10 This relation is quasi-linear. However, if the cross product is negated, this relation can also be seen to be linear, since then the formula is defined as:

$$M = I_v \dot{\Omega} \tag{3.30}$$

The relation between $\dot{\Omega}$ to Ω is still linear, since it is an ordinary first-order derivative equation.

The relation between Ω to η can be nonlinear. Recall from Section 3.5 that for the definition of attitude angles, both Quaternions and Euler angles can be used. A rotation matrix is used in both cases to convert angular rates to angles. If Euler angles are used for feedback, the rotation matrix is nonlinear. This is due to (co-)sines in the rotation matrix. If small angles are used, this nonlinear effect is minimal. Multirotors are usually controlled around an equilibrium attitude state, and therefore small angles are used.

In the case of multirotors, it can be concluded that both the dynamics and the kinematics can be approximated as a linear system with minimal approximation error.

4

Cooperative aircraft

In WWII the US Air Force developed the F-82 Twin Mustang airplane. See Figure 4.1 [41].

Figure 4.1: Drawing of the Twin Mustang [5].

This airplane looks an awful lot like two of the same F-82 mustang airplanes being sown together, which is what happened in simple terms. The goal of this twin-fuselage design was to improve endurance. Although the airplane had two cockpits, it only used one for (manual) control. Various forms of these twin-fuselage airplanes have been developed. However, they all share the commonality that they are developed for better aerodynamic/endurance properties, and they are usually designed symmetrically along the longitudinal axis for ease of manufacturing [42]. So although one can see two airplanes being connected, the joint structure is being completely controlled from 1 position.

This Chapter will cover various forms of cooperative aircraft. Firstly, formation flights is researched, where the aircraft are not physically connected. Then Air-to-air refuelling is mentioned, which can be seen as a hybrid between physical connection and formation flight. Thirdly, the section on swarming will explain various forms of cooperative flight where each aircraft has a similar decision-making role as opposed to the standard form of formation flight. Next, mid-air (dis)assembling multirotors is covered. Here the multiple modules are physically connected to each other mid-air. Lastly, the in-flight release of aircraft is researched. Throughout the Chapter, emphasis will be placed on the (relative) control strategies and the forms of intercommunication between the aircraft.

4.1. Formation flight

In formation flight, the airplanes need to be close, flying at a constant relative position. Different forms of formation flight exist; The closer the formation, the less room for the different aircraft to move around. Closer formation flights are generally harder for that reason. The decision-making process in formation flight is crucial; What information is vital for the pilot to fly safely in a formation? Different aspects of formation flight will be discussed in this section. Firstly manned formation flight is discussed, and later unmanned formation flight will be discussed.

Formation flight dates back since the beginning of manned flight and has served various purposes. This ranges from tactical advantages in war scenario's, demonstrations to aerodynamic advantages

when flying in formation. Most of the research these days on formation flight has to do with performance advantages. It has been proven that the air wake of an aircraft can create fuel savings for the following aircraft. This counts for both fixed-wing aircraft as well as rotorcraft [43].

In the thesis-work of C.A. van der Kleij, a controller was designed for the B-747 airplane to aid in formation flight [44]. He created a more elaborated controller and had as well calculated the economic benefits of flying in the wake of other aircraft. In terms of sensors, van der Kleij mentioned that accurate relative position knowledge is required. Currently, the standard B-747 aircraft is not equipped with such sensors. Sensors that would be able to perform this task well can either be a Doppler radar, laser ranging or (Differential) GPS. Also, a stable data link would be required between the different aircraft. In order to have the lowest fuel consumption, the aircraft must fly in the wake vortices of the aircraft in front. A LIDAR system could be used to find this sweet spot. This has been proven feasible [45].

Individual roles in formation flight

In formation flight, it is imperative to have a clear understanding of the various individual roles have in the formation. Most manned formation flights use a leader-follower role. In this way, the flight leader takes on all tactical decisions, and one or more wingmen follow its lead. See Figure 4.2 for an example of this topology.

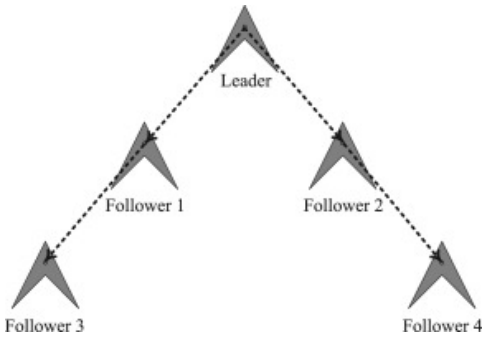

Figure 4.2: Topology of a leader-follower formation flight [6].

The flight leader needs to know what flight path will be flown. This flight path can be pre-planned or determined in-flight, but the flight leader requires knowledge of its position to compare its current state to the desired one. The wingmen require merely knowledge of the relative position. The wingmen, therefore, require other information for their control decision making. In this way, the flight leader takes care of all the high-level decisions, while the wingmen have to deal with a lower level of decision-making. Since the beginning, the leader-follower role has been the standard for manned formation flight.

One of the reasons is the following; Picture a situation where two different airplanes try to fly next to each other in a lateral manner. If both planes are too far from each other, they will steer towards each other. When they are too close, they will both steer away. This is mentioned as an ”accordion” effect [46]. This effect can be prevented by deciding one would be the leader of the group and the others to be the wingmen.

Furthermore, a leader-follower role can mean that the wingmen aircraft can be equipped with fewer sensors than the leader since a lower decision-making level also requires less knowledge of its states. For example, if a leader is flying at 400 knots ahead of the formation, the wingmen will also need to fly 400 knots to stay at a relative position. However, the wingmen will not look at the airspeed sensor but merely at the relative position of its aircraft to the leader.

The leader-follower role division is not the only option for successful formation flight. Formations can be flown using a strategy without a leader. Section 4.2 will elaborate more on this particular behaviour.

Air-to-air refueling

Air-to-air refuelling is a special case of formation flight. This formation is special because a refuelling boom needs to be positioned between the two airplanes to refuel one properly. This means that a physical connection between the two aircraft is made in formation flight. In order to achieve this, the

relative position needs to be constantly known. Vision or other sensors is usually used in these cases. Being the bigger aircraft, the tanker will try to fly stable in a specific course, and the other airplane will put in minor steering adjustments to have the proper relative position. The tanker plane takes on the leader role for formation flight in this case.

The research of Captain Steven M.Ross covered autonomous formation flight control in an air-to-air refuelling scenario [7]. Air-to-air refuelling occurs by performing different formations in succession. These formations are shown in Figure4.3. The path of the arrow shows the sequence after refuelling has been accomplished. This order is reversed if a follower aircraft wants to get in the position of refuelling. The number under the four formation positions represent the Formation position offsets between the GPS antennae of the tanker and the follower. The offset is defined in feet for the X-axis, the Y-axis and the Z-axis, respectively.

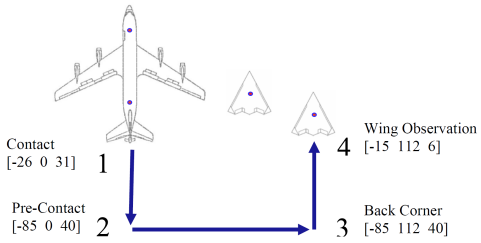

Figure 4.3: Formation positions and Position change paths [7].

Ross created a complete simulation between two aircraft in Simulink. One aircraft would function as the tanker and has the role of leader. The other aircraft is to be refuelled and has the role of follower. In order to verify the results, Ross mentioned acceptable tolerances. This is not defined in literature since this is very much situation dependent. For the contact position, the tolerances are more clear. In this formation, the follower aircraft is being refuelled and therefore has a physical boom between the aircraft and the tanker. This refuelling boom can not operate at any angle and has its limit. Figure 4.4 shows these limits. If these limits are exceeded, the boom will automatically detach to avoid a collision. The refuel boom envelope is defined as a performance goal.

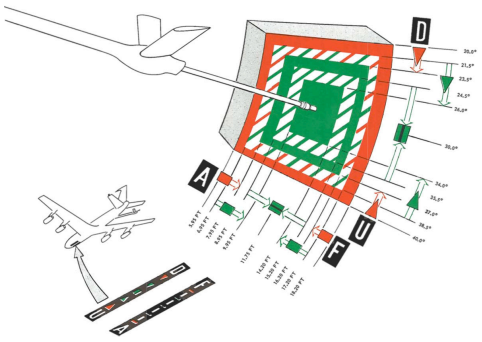

Figure 4.4: Operating limits of the refueling boom [8].

In human air-to-air refuelling, the follower aircraft and tanker are constantly communicating. The tanker is giving corrections to the follower, while the tanker aircraft tries to fly as predictable and stable as possible.

Heading angle (ψ), pitch angle (θ), bank angle (ϕ) and roll rate (p) information is sent to the wing aircraft, originating from the lead aircraft's IMU. Differential GPS, DGPS, is used to determine the relative position. The wing aircraft then performs a coordinate transformation and calculates its aircraft commands using PI control. In order to make the simulation resemble reality, disturbances to the communication were added. This includes time delay, sampling error and noise. The simulations looked promising, with the wing aircraft flying within the boundaries of the formation. Even in situations where the tanker would make a 30 degrees bank turn, the follower aircraft would be able to follow it.

Real-life testing, however, showed the importance of communication between the leader and the follower aircraft. GPS estimation errors and drifting heading information caused the follower aircraft to

fly out of the boom envelope in the contact formation position during the 15 degrees and the 30 degrees bank turn. Apart from disturbances, Ross also mentioned that the integrator in its PI controller could be turned off in critical moments. In case of a faulty communication error, the integrator counts up the error in the turn, causing an overshoot when the tanker is ending the turn.

Formation flight for UAV's

The previous section mainly mentioned manned formation flight. But, like the general control theory, a comparison can be made between manned and unmanned formation flight. Computation of the human pilot now has to be done by flight computers. The choice of sensors is vital; What does the pilot, or a flight controller, need to know in order to make the proper control decisions? Since the same aerodynamics properties still apply, arguments can be given that a leader-follower relation between the different pilots seems to be straightforward to implement. This means that the leader will require different sensors than the follower. However, there are cases where the follower can also have the same sensor as the leader. This can be in the case of redundancy; The leader can malfunction, and then (one of) the follower(s) can take over. Another case can be swarming. This will be covered more in-depth in the next section.

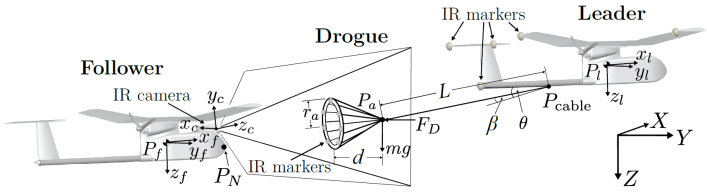

Figure 4.5: Set-up for airborne docking of 2 UAV using IR data [9].

A team in Australia investigated airborne docking using strictly UAVs [9]. Wilson et al. propose an inventive way for the follower to acquire the information for a successful formation. The back of the leader aircraft and the drogue were equipped with Infra-Red, IR, markers. See Figure4.5. Using an IR camera on the follower aircraft alongside known geometry of both the leader aircraft and the drogue, relative position to the drogue (and the leader) can be estimated. This alone would imply a way of formation flight, where the follower aircraft would not need to communicate to the leader. However, Wilson et al. also has the leader aircraft send its current state to the follower. This information would then be fused using an unscented Kalman filter with the IR data on-board the follower aircraft to have a better relative state estimation. This approach proved to be prone to signal noise very much. Also, a separate Formation flight computer (FFC) is required to perform the relative state calculations. This information from the FCC is fed to the autopilot, calculating the actual control commands.

Another example of a formation flight control system for UAVs is proposed by Zdzisław Gosiewski et al. [47]. He derived a PI controller for a V-shape formation flight. The role division is again a leader-follower one, and the leader sends out signals to the wingmen containing reference trajectory. The follower UAVs then use the reference trajectory alongside the relative position and velocity of the leader to make their own control decisions.

It has already been mentioned that one of the main benefits of formation flight is fuel consumption. This is due to the wake vortex effect. Research in 2002 has proven that the benefit can even reach a fuel consumption reduction up to 34% [48]. This is due to the decreased drag coefficient on the trailing aircraft. The wake vortex effect is not consistent around the aircraft, and a sweet spot exists where the biggest drag reduction is found. Varying per aircraft also the sweet spot is not consistent for the full flight envelope. Brodecki et al., therefore, developed a flight control system using the sensing of this sweet spot estimation [49]. The sweet spot for maximal drag reduction can be found by measuring the wash-up coefficient. Measuring the sweet spot in-flight serves a dual purpose; First of all, to fly in formation for saving fuel, it is better to estimate the sweet-spot on-board instead of knowing the exact relative position beforehand. This is due to the changing place of this sweet spot during the flight envelope. Secondly, Brodecki et al. proposes a control system that requires less information from the leader aircraft to stay in formation. In other researches, the follower required full state knowledge of the leader in order to know its relative position [50]. Brodecki et al. only required the relative velocity of the leader aircraft alongside the followers' measurements, including the wash-up coefficient estimation

4.2. Swarming

So far, only formation flights with a hierarchic topology are mentioned. Formation flight can also be possible where the higher level decision-making is made by the group in a more equal manner. This is referred to as swarming. Swarming is not new; Insects and other animals have been flying in swarm formations for centuries. An example is bird flocking behaviour. This flocking behaviour could be simulated with the Boids algorithm in a simplified form. This algorithm is based on three primary rules:

1. **Separation:** Boids move to avoid colliding with each other.
2. **Alignment:** Boids steer to match the average direction of the baround them.
3. **Cohesion:** Boids move towards the centre of the Boids around them.

Figure 4.6 displays a visualisation of the three ground rules for the Boids algorithm. In the Boids algorithm, each of the individual nodes will go through the same rules and together, they can fly as a whole without collision. This, in essence, is swarming, and this section will cover research in which this decentralised control has been developed for UAVs.

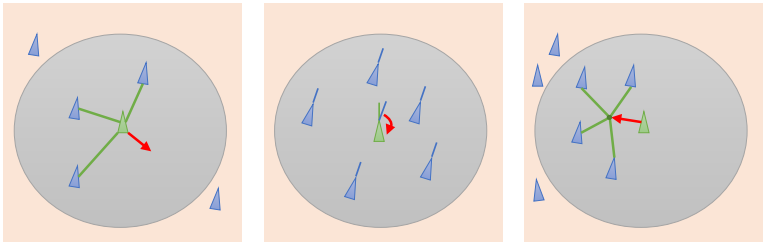

(a) Separation (b) Alignment (c) Cohesion

Figure 4.6: Three ground rules for the Boids algorithm.

Arshad Mahmood et al. proposed a decentralised formation flight control for quadcopters [51]. This was achieved using robust feedback linearisation. In this case, no significant approximation error was found while linearising the nonlinear dynamics of the quadcopters. Mahmood et al. proposed a two-layer control system for the formation flight. The feedback linearisation in the inner layer and a linear formation control law in the outer layer. In order to make the feedback linearisation more robust, a sliding-mode compensator is added. The sliding-mode compensator behaves as an observer and has the function of estimating disturbances and high-order state variables [52]. In this way, a form of swarming can be achieved.

Simulations have shown that multiple quadcopters can rearrange themselves in different formations. However, in order to achieve this, accurate knowledge of 3-dimensional positions and a heading is required to be known. Mahmood et al. mentioned in the concluding remarks issues that still required attention, including communication link failures between quadcopters. Also, any collision avoidance algorithm was not yet implemented in the system.

Ruibin Xue et al. proposed a decentralised formation flight control of a multi-UAV system with communication constraints [53]. The communication constraints are defined as a time delay of the communication between the various UAVs. The time delay results from all the different steps it takes for information to be processed on another aircraft. Their paper aims to have a formation of UAVs fly along a predefined track and in a predefined formation shape. This means that the desired distance between each of the different UAVs is pre-calculated for each of the different UAVs. The communication between the different UAVs is done in a novel matter. Xue et al. proposed a constant changing topology. This means that each UAV communicates with just one other UAV each time. Then, each iteration, different UAVs will be communicating to others to communicate with all the other aircraft eventually.

The proposed way of communication was using a consensus protocol. The consensus protocol for formation flight, previously proposed by W.Ren (2007) and Seo (2009), is a communication protocol where the information is checked before using it [54, 55]. For example, if UAV 1 were to send its states to UAV 2, UAV 2 would first check if the states are within acceptable boundaries to use its neighbour's states as input for its own control decisions. Simulation proved this method to be feasible. The time delay between the different UAVs has been implemented and was non-uniform, meaning that different

UAVs were communicating with different time delays. However, the paper acknowledges that collision avoidance was again not taken into account, just like the paper of Mahmood et al.

A paper that proposes a control model including collision avoidance is the article by Zhou Chao et al. [56]. The model is designed using nonlinear model-predictive control. The formation uses a general virtual reference point. This virtual reference point has a certain position and velocity such that the others will refer to it as if it were the leader in the formation. The formation can avoid collisions as a group but also between each other using a cost function. Simulation has also proven this to be reliable. However, this paper proposed that future work should include communication constraints and formation reconfiguration problems. This means that they have tested it with just one configuration and have not researched possible problems with communication restraints.

Matthew Turpin et al. proposed a formation control algorithm for UAVs, but in this case, particularly for aggressive trajectories [57]. Under this scenario, the communication uncertainties (such as noise and delays) can be disastrous. They propose a form of consensus protocol but to all neighbouring UAVs. The formation, in this case, has a leader again, but the other UAVs do not calculate their control input with reference to the formation leader only. Also, all their neighbours are taken into account. In this case, it is more of an indirect leader-follower communication strategy. In their experimental research, however, Turpin et al. analysed the behaviour of the formation in the case of degrading communication between the UAVs and in case one of the UAVs completely fails. For their experiments, MATLAB in conjunction with ROS was used. A central computer sends the trajectory commands to the individual robots. This centralised control method is used to simulate a decentralised control method. Calculations on the ground computer are made so that the individual robots have no global knowledge of the whole structure. The inputs are sent at 50Hz using wireless communication. The robots themselves then solve the control input necessary for their actuator to follow the desired trajectory. Experiments have proven that the error of their relative trajectories seems to stay very low, even in the case of degrading communication.

4.3. Physical connected UAV's

Distributed Flight Array

In the field of multirotors, physical (dis)assembling UAV's have also been researched. Researchers at ETH Zurich have developed the Distributed Flight Array, DFA [10]. See Figure 4.7. This modular platform consists of single rotor units that would not be able to fly by themselves. They need to work together in order to fly. The different nodes would drive in a coordinated way and make a predefined shape. This shape would then be able to fly. All possible connection patterns have been run in the simulator, and the control parameters have been determined beforehand. The nodes communicate with the other nodes in a distributed manner. This would simplify and create a more reliable communication stream between the different nodes. Also, less bandwidth of communication is required.

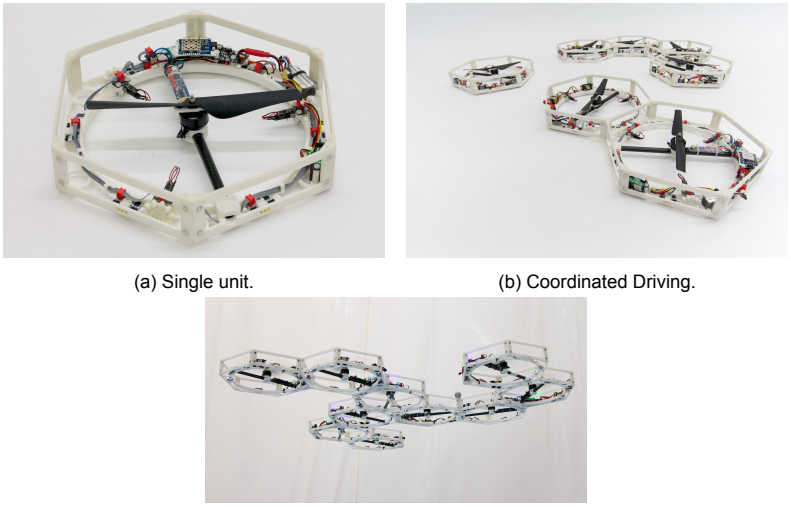

(a) Single unit.

(b) Coordinated Driving.

(c) Coordinated Flight.

Figure 4.7: The Distributed flight array: three stages [10].

For the control strategy, a new parameterised controller was developed. The calculated output of the controller is defined as:

$$u_d = Q \begin{bmatrix} f_z \\ f_\gamma \\ f_\beta \\ f_\alpha \end{bmatrix} \tag{4.1}$$

,where the different DOF each are calculated to work as a second-order mass-spring-damper system individually, defined as:

$$f_z = -Nm(2\omega_z\zeta_z\hat{\dot{z}} + \omega_z^2(\hat{z} - z_d)) \tag{4.2}$$

$$f_\gamma = -I_x(2\omega_\gamma\zeta_\gamma\hat{\dot{\gamma}} + \omega_\gamma^2(\hat{\gamma} - \gamma_d)) \tag{4.3}$$

$$f_\beta = -I_y(2\omega_\beta\zeta_\beta\hat{\dot{\beta}} + \omega_\beta^2(\hat{\beta} - \beta_d)) \tag{4.4}$$

$$f_\alpha = -I_y(2\omega_\alpha\zeta_\alpha\hat{\dot{\alpha}} + \omega_\alpha^2(\hat{\alpha} - \alpha_d)) \tag{4.5}$$

ω is defined as the natural frequency, ζ the damping ratio, Nm is the total mass and I is the inertia. γ, β, α yield the Euler angles, z is a predefined altitude, the hat superscript denotes an estimate of the state and $\ldots_d$ denotes the desired state.

Equations 4.2-4.5 in essence explain the closed-loop dynamics in each of the DOF. The Q matrix divides the desired input for the total system into the input for each of the individual nodes. Full state feedback is then used to complete the controller.

The researchers mentioned that this parameterised linear controller is not the most optimal, but it gave them a good insight into how the dynamics changed with the different configurations. Furthermore, the parameters for the different configurations could be relatively easily calculated, giving them more freedom to experiment with different configurations. In simulations, the parameterised controller was compared to an optimal H_∞ controller, and their parameterised controller did perform worse. However, given their controller's ease of implementation and scalability, their parameterised controller was still more feasible.

During MATLAB simulations, the DFA was controlled in a decentralised manner. Each node has to make its own control decision based on its sensors. These sensors consist of an IMU and an IR distance measurement unit. The DFA uses the information of the various IR distance measurements of the different nodes to improve the state estimation of the whole structure. This method is called distributed tilt estimation. Estimating the states using purely gyroscopes was investigated to be noisy and therefore not super reliable. This is mainly because gyroscopes perform well in the short term, but drifting can occur in the long run. Following this form of tilt estimation, each module only requires the height information from the adjacent modules/nodes. The gyro information is then fused with the tilt estimation. The researchers also mentioned process noise and measurement noise and proposed ways to deal with it. Measurement noise includes time delay, together with signal and process noise, which is referred to as physical aerodynamic noise. Process noise results from the turbulent flow due to the rotor's spinning and other aerodynamic characteristics of the structure.

In the practical experiments of the DFA, the platform was being controlled with an off-board vision system, and some of the control calculations were also performed off-board. They obtain attitude states from the rate gyroscopes, but they obtain the position states from a 3D motion capture system. This is necessary since the DFA does not have a global position system GPS or machine vision. The communication is demonstrated using a user datagram protocol (UDP). Checksums are performed in order to filter communication errors. During experimentation, the communication of the DFA has been described as unreliable but frequent. For outdoor experiments, a joystick was used to control the roll and pitch angles and yaw angular rate. A single set of control parameters was used that deemed feasible for all flight configurations.

Modquad

The University of Pennsylvania developed a somewhat similar design as the DFA, called the Modquad [11]. See Figure 4.8. The main difference is that the individual units can fly by themselves, so (dis)assembly can be done in-flight. The assumption during mid-air assembly is made that the shape

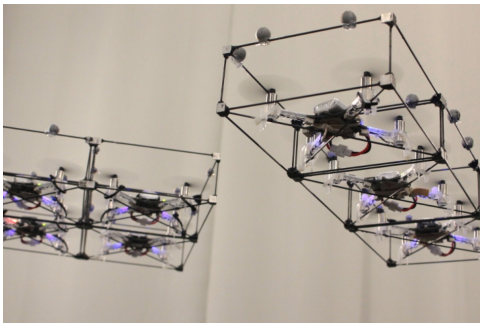

Figure 4.8: Modquad [11].

and relative location are known for each node. For their decentralised approach, the desired attitude and thrust is sent to the joint structure. The nodes themselves are then required to perform onboard calculations to calculate the control input. The input is calculated using a PD controller, see Section 3.2. Note that the integral part of the PID controller is not used. In all configurations, the PD gains can also stay the same. This has proven to be not the optimal tune for every configuration, but it performs well enough in every situation.

A notable difference with the DFA is that every node is a quadrotor. This means that every node has four rotors and can keep its attitude, as mentioned in Section 2. Another difference has to do with actuator saturation. The DFA developed their controller so that the force applied, to achieve a particular moment around equilibrium, is proportional to the distance with respect to the C.G. The result was that actuator saturation occurred on the nodes far from C.G. The Modquad tried to minimise individual actuator saturation by controlling all of the actuators in a particular quadrant with the same magnitude. This way, the desired force is more equally distributed to the different actuators. The downside is that this method is not energy efficient.

An individual node will always approach the joint structure for the docking sequence, which is comparable to the approach of air-to-air refuelling in a leader-follower role. Once a module is docked to another module, a central vision position tracking system, VICON, detects this occurrence and uploads new parameters to each module in the structure. These parameters include the total configuration of the system and the relative position that each of the nodes has to one another.

During the experiments, the Modquad used off-board processing for position estimation of the units. Therefore, the total system constantly got attitude commands sent to each of the nodes.

Also, motor saturation still occurred despite their effort to minimise it. The main reason was a relative lack of yaw authority. This means that the motors have a relatively hard time using the reaction torque with the increased inertia of the bigger structure. Their recommendation is to minimise the control gains on the yaw axis, so it will not take up such a significant part of the control authority of the actuators.

Disassembling Modquad

The Modquad opened possibilities for more research, and David Saldana et al. developed a new version of the Modquad that is able able to self-disassemble in-flight [12]. The individual modules are held together by bigger magnets compared to the previous version of the Modquad. As shown in Figure 4.9, two modules can separate by creating an attitude angle away from each other. This is referred to as torque peak generation. Since both modules are angled away, this generates a net force outwards, overcoming the magnet's force in its turn. For the experiment, the size and type of magnet were carefully chosen so that accidental separation would not likely occur, but torque peak generation would be sufficient for release. For the experiments, VICON measured the position of the different modules and their joint configuration and constantly sent those states to the different modules. The torque peak generation and the attitude control calculations are performed in each of the individual modules. If separation occurred between two parts of the original structure, an off-board computer updated the modules with the parameter for the new situation. This is performed in a similar way as mentioned in the original Modquad research [11].

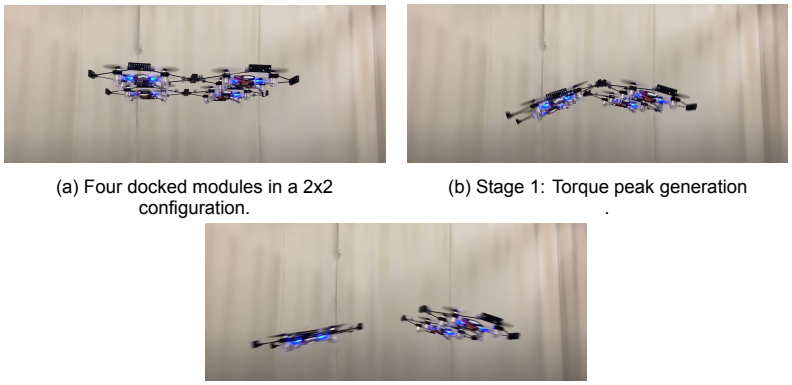

(a) Four docked modules in a 2x2 configuration.

(b) Stage 1: Torque peak generation .

(c) Stage 2: Separation.

Figure 4.9: Modquad disassembling in two stages [12].

4.4. In-flight release of aircraft

In this section, different options for mid-air released airplanes are specified. As opposed to the disassembling Modquad, in-flight separation is most of the time performed in a form where a bigger aircraft is releasing a smaller aircraft [11]. For example, Tony S.Tao et al. developed an In-Flight-Deployable Micro-UAV [58]. The main goal was to minimise the aerodynamic cross-section of the aircraft before release. In Section 2 it became clear that a fixed-wing aircraft needs wings in order to generate lift. But, these wings are perpendicular and to the fuselage and are relatively big compared to the fuselage. An aircraft that folds up would solve this issue. Other examples of these morphing UAVs capable of launch include the Squid [59], the Altius 600 [60], the Gremlin [61] and the Dash X [62]. See Figure 4.11.

A less aerodynamic optimised approach is researched by Seunghwan Jo et al. [64]. They propose an integrated system of a quadrotor and a conventional fixed-wing aircraft. One could say that this system would resemble a quadplane, and in the geometry, it would be. However, the fixed-wing aircraft carries the quadrotor on the top but does not use the VTOL capabilities of the quadrotor. Their motivation is to use the agility of the quadrotor at a specific location but will only use the performance of the fixed-wing to get to that location. The in-flight deployment happens as follows: The fixed-wing aircraft will pitch up, and a release mechanism releases the quadrotor using a servo system. Due to the drag forces, the quadrotor will fall away from the fixed-wing aircraft and enter a free-fall state. The quadrotor will then re-initialise its flight computer and recover its quadrotor angle by angle. The quadrotor will then autonomously fly to a designated waypoint.

An approach a little similar, but then the other way around, is proposed by Insitu [65]. Insitu developed the ScanEagle, a fixed-wing UAV, widely used by various military forces, even in Naval applications. But, because a fixed-wing aircraft requires forward speed for lift, the ScanEagle requires a launch catapult and a recovery rope to take off and respectively land. This creates extra logistics to operate the ScanEagle. Therefore a Flying Launch And Recovery System, FLARES, was developed. This is, in essence, a giant quadrotor that will vertically take off with the ScanEagle underneath it. Once in the air, the ScanEagle will be dropped and, due to its altitude, gain enough forward speed to get into stable forward flight. FLARES can also provide a solution for in-flight recovery of the ScanEagle; The quadrotor drops a rope, and the ScanEagle will fly in that rope with a hook at the end of its wingtip similar to the ground-recovery system. After the ScanEagle is caught in the rope, the quadrotor will fly back to base. Once it has reached the determined position, it will slowly descent, carefully putting the ScanEagle to the ground.

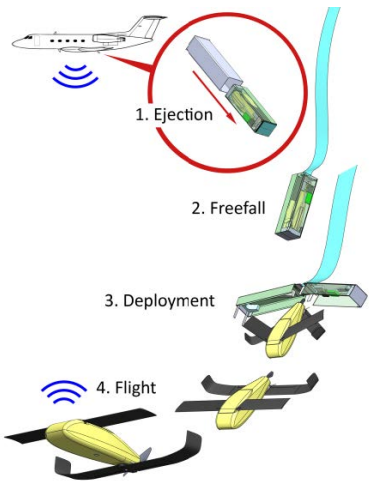

(a) In-Flight-Deployable-Micro-UAV deployment sequence [58].

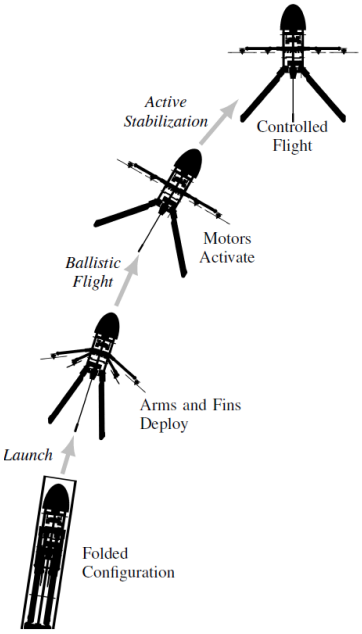

(b) SQUID deployment sequence [59].

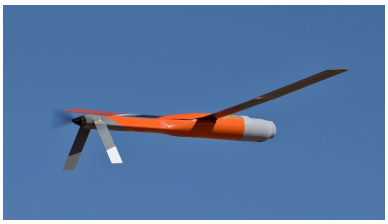

(c) ALTIUS-700 [63].

(d) GREMLIN [61].

(e) DASH-X [62].

Figure 4.10: Representable examples of in-flight deployable UAVs.

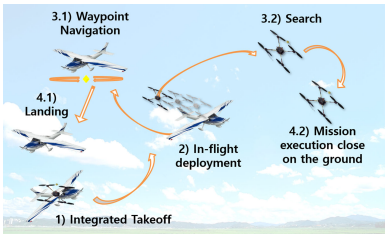

(a) Concept of operation for a fixed-wing UAV to deploy a multicopter UAV in-flight [64].

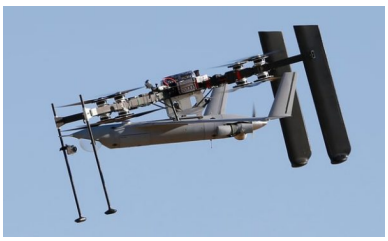

(b) FLARES [65].

Figure 4.11: Combination of rotorcraft and fixed-wing for in-flight release.

5

State of the art review

In Chapters 2 through 4 of the literature study, different subjects have been covered that are relevant for the research objective. This section will analyse what part of the research objective has already been answered and what is still required to be researched.

Physical design

Different forms of aircraft types have been discussed in Chapter 2. The goal of this research is that all of the aircraft forming a joint structure would contribute to flight. Furthermore, the aircraft would require both endurance and agility. One option would then be to develop a quadplane design where both aircraft would contribute to flight. This design could come close to the research by Seunghwan et al. [64]. In this case, the connecting system between the two aircraft still remains to be researched. Seunghwan et al. did not use the VTOL capability of the quadcopter. From observations, the release mechanism would not be able to hold the full weight of the plane with the addition of the force that the quadcopter requires to perform a positive lift.

Another option would be to build upon the Nederdrone design [2]. This tailsitter platform can perform both forward flight and VTOL/hover in a multi-redundant manner. For the in-flight disassembly, a couple of the actuators would be able to release in-flight. This option would agree with the given research constraints and would serve the research objective. Figure 1.1 already reveals that this concept was chosen. A few benefits exist in favour of the Nederdrone design.

First of all, a quadplane is known for the fact that in either hover or forward flight, not all actuators would be utilised. In hover, the forward propulsion is not used, and in forward flight, the actuators of the quadrotor are not used. In the case of the tailsitters, all actuators are used across the whole flight envelope.

Control

The next chapter of the literature study revolved around the control theory of aircraft. In particular, two main control theories have been covered: PID and INDI. PID is the most popular control theory used in the vast majority of different UAVs. Different forms of PID, like PD or PI controllers, have proven to work for different circumstances. PID has not proven to be the most robust controller for hybrid aircraft. Other control methods solve some of these issues, and (I)NDI is one of these control theories. Using the tailsitter platform, the aircraft requires a fast and robust control method. NDI is a model-based controller instead of PID, given that the system dynamics are known. This is difficult to determine accurately, and therefore INDI posed an excellent alternative. This sensor-based controller can cope well with uncertainties due to its robust nature. The research objective deals with not one but two aircraft. From research, joint operations between aircraft cause further uncertainties like communication time delay and information mismatch. A robust controller is therefore arguably more important. For all those reasons, INDI is chosen for the general control method. An unsolved question is how the integrated control theory is defined. Will both aircraft be controlled with INDI, or will one of the two aircraft require a different form of controller? This remains to be investigated and has not yet been answered in literature for a joint structure.

Different control modes have also been discussed. Depending on the type of mission, different control modes are required. The joint structure will eventually be necessary to fly beyond line of sight. This would then rule out mere attitude control since way-points have to be flown. This means that for the first two phases of the mission, take off/hover and forward flight, the joint structure needs to be able to follow a way-point mission. Once at the desired location, the two aircraft will separate, and the bigger structure will loiter above the quadrotor, and the smaller aircraft will carry out its mission. Like the controller, it has yet to be researched which aircraft will have what mode in the joint configuration that must be flown. In any case, the joint controller has to adhere to a position controller somehow.

Cooperative flight

Chapter 4 explained all forms of cooperative flight. Quite a bit of research has been performed in this field, but also the biggest research gap exists in this area. First of all, different kinds of formation flights are discussed. Although some researchers have been pushing the limit of how tight a formation can be, all aircraft always had a separation distance. Even a somewhat physical connected formation flight, namely air-to-air refuelling, has proven to be forgiving in case the operating limits are exceeded. Instead of a crash, the refuelling boom automatically detaches, allowing for safe separation. The physically connected joint structure implies a different form of formation flight. There is no chance for collision since both aircraft are already attached to each other. This means that an accordion effect will have another influence on the joint structure, and this is yet to be investigated.

Every form of cooperative flight has used a form of communication. This ranges from decentralised control input to each of the different nodes in a formation to a mere position of a leader aircraft for relative distance measurements. The communication is, however, far from perfect. Researchers have been simulating different challenges that come with communication. Different communication typologies for a multitude of aircraft have been investigated, and the simulated physical constraints of communication have been taken into account. This includes time delay, false information and noise. Although most research had taken the constraints of communication into account, none were critically difficult to overcome. Still, it has always been defined as a challenge. Suppose a joint control strategy would not require sharing information between the two aircraft; these challenges would not have to be considered. It would take away one point of failure. For this reason, this constraint was added to the research objective. Cooperative flight without any intercommunication is new, and therefore research should also be performed in this area.

In the case of the DFA, constant communication between the different nodes is used and is even vital for flight. Their form of communication is a physical one, using a UART connection between the different nodes. One of the states that is being communicated is the height. This information is shared to better deal with state estimation errors from the sensors. They perform attitude control decentralised, but they get the attitude reference states from an off-board computer. This is due to the lack of an onboard position estimation system. In the case of the proposed joint structure, both aircraft will be equipped with a position estimation system in this report. Also, the distance between the ground station and the aircraft is too big to get reliable attitude reference information. The attitude reference states have to be transmitted at a too high rate for the allowed bandwidth at that distance. The Modquad also used a form of decentralised control, with a vision system taking care of the position estimation. Again, this is not possible for this research due to an unreliable data connection over long distances.

In-flight release/disassembly

At the beginning of this chapter, the release methods have been mentioned slightly. Sections 4.3 and 4.4 show what types of in-flight release mechanism exist already. All cases mentioned in 4.4 have a bigger aircraft drop the smaller aircraft except for two quadplane versions [64, 65]. This implies that the bigger aircraft has to carry ”dead weight” from point A to B. Even for the quadplanes, one part of the total structure contributes to flight at any given time across the whole flight envelope. The quadrotor did use its VTOL capabilities with the quadplane design of Seunghwan et al.; this is the case with the FLARES project. But for the FLARES project, the quadrotor merely releases the fixed-wing aircraft at an altitude, and the two aircraft do not travel together to another location. Instead, the quadrotor waits at a certain position in order to catch the fixed-wing aircraft, after its mission.

The DFA and the Modquad are both joint aircraft structures that work together to maintain flight. The DFA in its current version is only able to assemble on the ground and is not able to disassemble in-flight. The Modquad is able to both assemble and disassemble in-flight. The problem, however, is

that both the Modquad and the DFA consist of a multirotor design. Chapter 2 already proved that this would not provide the endurance required. A conventional full-size helicopter would be able to provide the endurance, but manoeuvring in the shed would then again be challenging. The Modquad nodes are connected by the use of magnets. This method works for the Modquad since the pulling and shear force between the nodes is relatively low. In the proposed concept from Chapter 1, the expected force is far greater, and therefore a new release system would be required.

In conclusion, for both airplanes and multirotors, flight with some form of physical connection have been researched or performed. However, the connection of an airplane and a multirotor with the purposes of disassembly mid-flight is novel. Also, the physically connected multirotors often rely on off-board computation, while this thesis research aims to do all computation strictly onboard.

III

Additional Results

6

Extra joint control strategies simulations

In the Scientific Paper, three joint control strategies are investigated and compared to a control group. In the preliminary work, these were not the only strategies that have been investigated. This section will cover two more control strategies, given the same measurement and reference model restrictions. The two control strategies will be compared to the control group and the angular rate damper strategy.

6.1. angular rate PD damper

The first strategy combines the angular rate and the angular acceleration damper strategy. In this case, the angular rate reference will still be set to 0 [rad/s] for the quadrotor and after it follows a proportional gain. Next, the angular acceleration measurements will be deducted, and another gain is added. This is comparable to the PD outer loop structure of the INDI attitude controller [4]. This will be referred to as the PD damper strategy. The control loop is shown in Figure 6.1.

Figure 6.2 shows the control group, the angular rate damper strategy, and the angular PD damper response for different P and D gain values. Important response parameters are listed in Table 6.1 and 6.2.

From Figure 6.2 the response shows very similar behaviour as the angular rate damper strategy if the product of the P and D values for the PD damper equal the P values of the angular rate damper. The control loop displayed in Figure 6.1 shows that indeed the signal values will get multiplied with the D gain after the input signal is multiplied by the P gain. The PD damper has no significant benefit compared to the angular rate damper strategy. As with tuning the angular rate damper strategy, a trade-off has to be made between increased performance with the step input or the step disturbance. This is a design choice. Results from the paper have shown that for the angular rate damper strategy, a proportional gain of P=400 yields overall improvement.

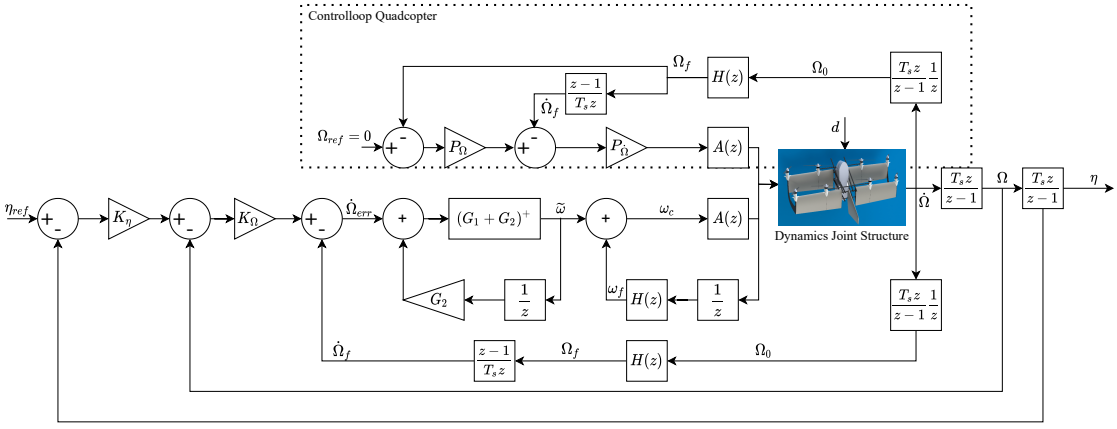

Figure 6.1: Control loop schematics - PD damper

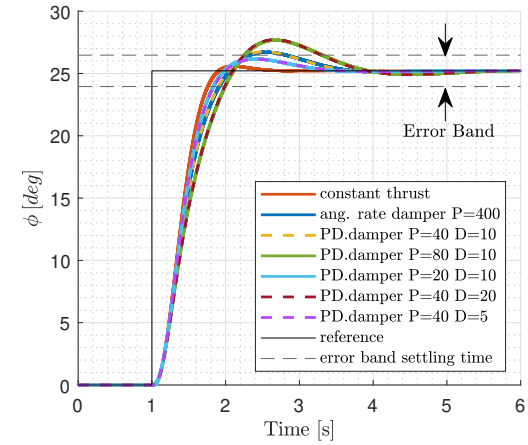

(a) PD damper Step Roll

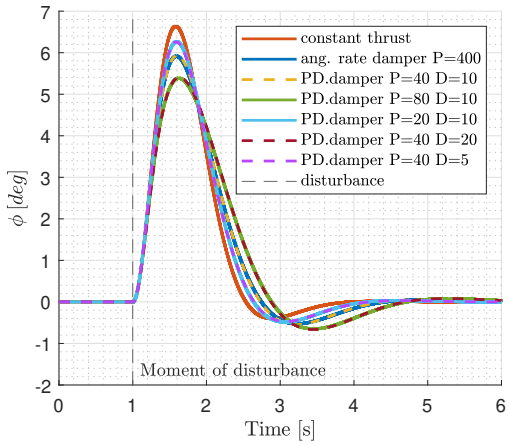

(b) PD damper disturbance roll

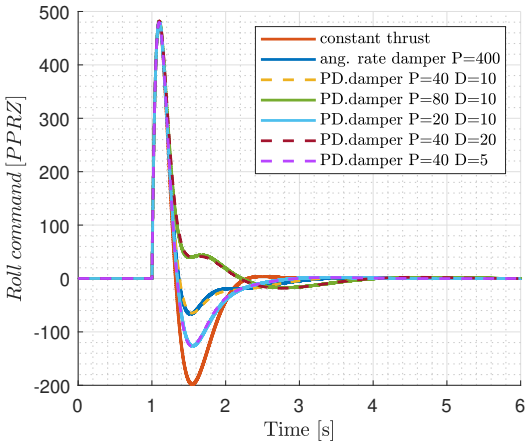

(c) PD damper Step CMD

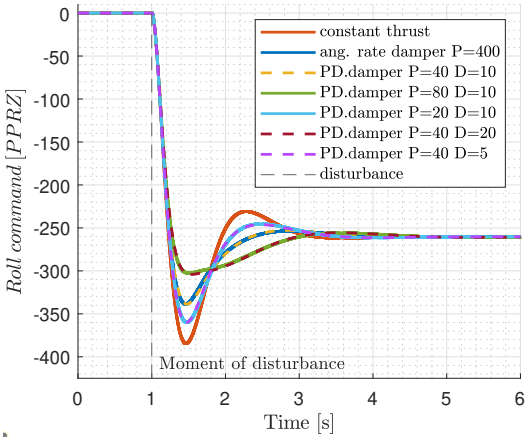

(d) Disturbance CMD

Figure 6.2: Step input and step disturbance response for different tuning values - PD damper

	Settling time	Overshoot	Max CMD	Energy required for t=[0-6]
constant thrust	0.76 [sec]	1.46 [%]	479 [PPRZ]	185 [PPRZ· s]
ang. rate damper P=400	1.82 [sec]	5.95 [%]	480 [PPRZ]	139 [PPRZ· s]
PD damper P=40 D=10	1.81 [sec]	6.10 [%]	481 [PPRZ]	143 [PPRZ· s]
PD damper P=80 D=10	2.31 [sec]	9.79 [%]	482 [PPRZ]	154 [PPRZ· s]
PD damper P=20 D=10	0.83 [sec]	3.81 [%]	480 [PPRZ]	165 [PPRZ· s]
PD damper P=40 D=20	2.30 [sec]	9.94 [%]	483 [PPRZ]	156 [PPRZ· s]
PD damper P=40 D=5	0.84 [sec]	3.69 [%]	480 [PPRZ]	163 [PPRZ· s]

Table 6.1: PD damper - step input

	max ϕ_{error}	Max CMD	Energy required for t=[0-6]
constant thrust	6.64 [deg]	384 [PPRZ]	1303 [PPRZ· s]
ang. rate damper	5.92 [deg]	339 [PPRZ]	1303 [PPRZ· s]
PD damper P=40 D=10	5.93 [deg]	339 [PPRZ]	1303 [PPRZ· s]
PD damper P=80 D=10	5.39 [deg]	303 [PPRZ]	1303 [PPRZ· s]
PD damper P=20 D=10	6.27 [deg]	360 [PPRZ]	1303 [PPRZ· s]
PD damper P=40 D=20	5.41 [deg]	304 [PPRZ]	1303 [PPRZ· s]
PD damper P=40 D=5	6.26 [deg]	360 [PPRZ]	1303 [PPRZ· s]

Table 6.2: PD damper - disturbance

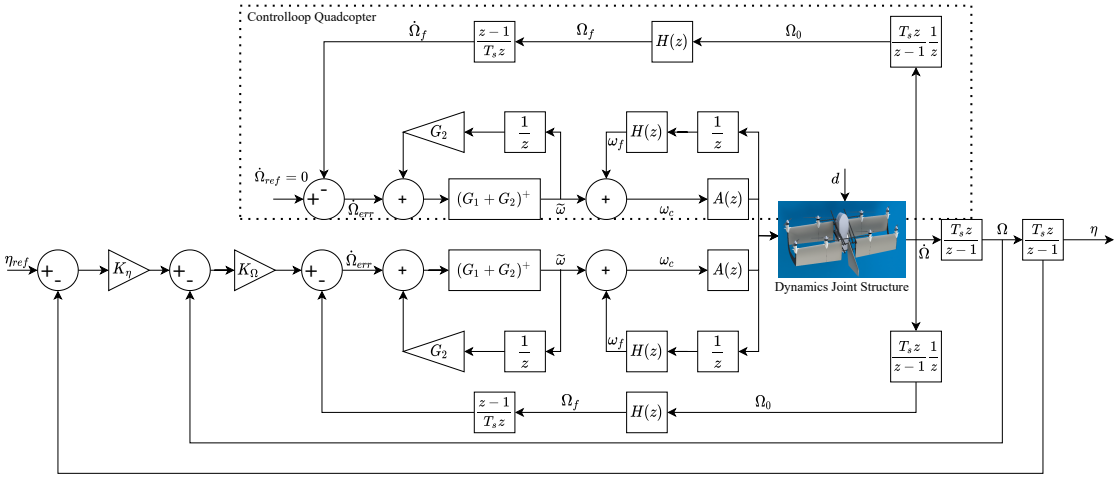

Figure 6.3: Control loop schematics - INDI damper

	Settling time	Overshoot	Max CMD	Energy required for t=[0-6]
constant thrust	0.76 [sec]	1.46 [%]	479 [PPRZ]	185 [PPRZ· s]
ang. rate damper P=300	0.88 [sec]	4.83 [%]	479 [PPRZ]	150 [PPRZ· s]
ang. rate damper P=400	1.82 [sec]	5.95 [%]	480 [PPRZ]	139 [PPRZ· s]
ang. rate damper P=450	1.91 [sec]	6.48 [%]	480 [PPRZ]	133 [PPRZ· s]
2INDI	2.15 [sec]	6.46 [%]	479 [PPRZ]	138 [PPRZ· s]

Table 6.3: 2INDI damper - step input

Due to the high similarity of the PD damper strategy to the angular rate damper strategy, this strategy was not selected for practical verification.

6.2. 2INDI damper strategy

The last investigated strategy is based on the existing INDI inner loop structure that is used by the biplane. This control strategy was also investigated because for the control group the joint structure uses the cascaded INDI control structure with all eight rotors. So ideally, the joint structure is controlled using the complete INDI architecture for all actuators. Chapter IV.A of the Scientific Paper illustrates that given the restrictions of this research, that is not completely possible. In order to keep as much as possible of the INDI architecture, an INDI inner loop controller for the quadrotor alongside the full cascaded INDI controller of the biplane is investigated. This strategy will be referred to as the 2INDI damper strategy. Figure 6.3 shows the complete control architecture of the joint structure.

If we recall Section 3.4, the virtual input, ν, is defined as the angular acceleration, and this is set as a constant 0 reference. Figure 6.4 shows the performance of the 2INDI control strategy compared to three variations of the angular rate damper strategy and the constant thrust strategy. Table 6.3 and 6.4 list the relevant response parameters.

The 2INDI control strategy shows an increased performance for disturbance rejection but a slower response for the intended step input. For disturbance rejection, the 2INDI control strategy reaches the maximum ϕ_{err} sooner than for all the other strategies. Nevertheless, it can be seen that further tuning of the angular rate damper strategy can also yield better results. Again, a trade-off must be made on how much one wants to decrease intended performance to have a better disturbance rejection.

Finally, the incremental nature of the INDI controller could be problematic due to integral windup [27]. For the same reason, the Integral part of a PID controller was not used in any other control strategy.

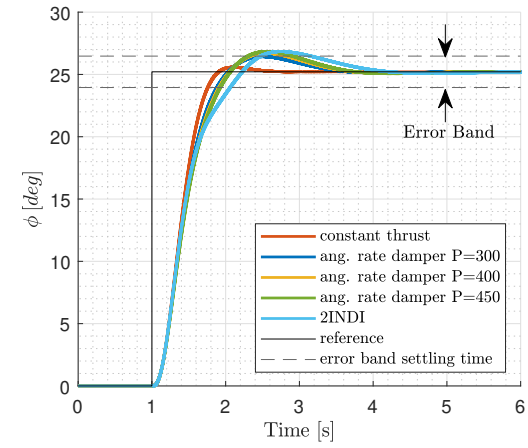

(a) Various strategies Step Roll

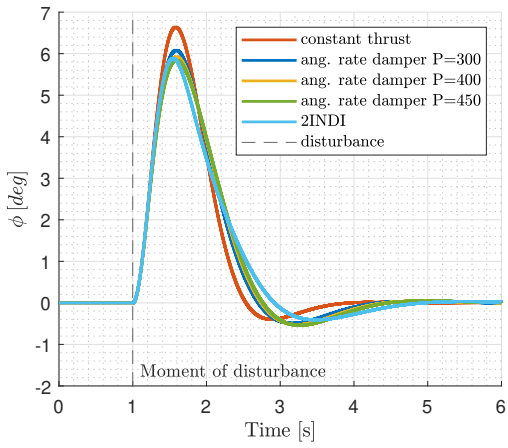

(b) Various strategies disturbance roll

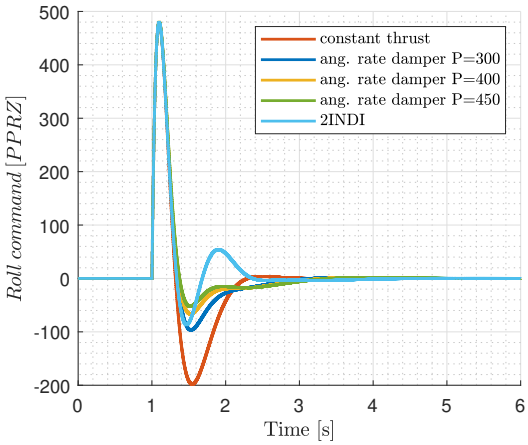

(c) Various strategies Step CMD

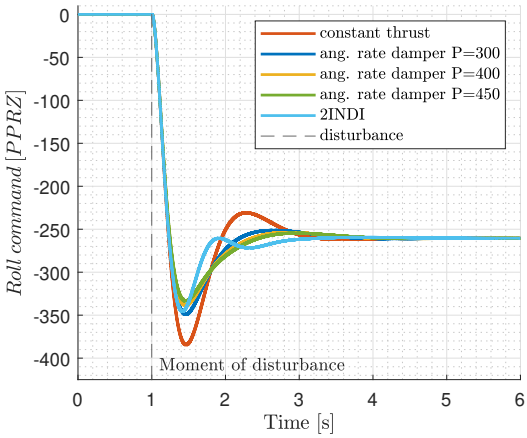

(d) Various strategies Disturbance CMD

Figure 6.4: Step input and step disturbance response for angular rate damper and 2INDI control strategy

	max ϕ_{error}	Max CMD	Energy required for t=[0-6]
constant thrust	6.64 [deg]	384 [PPRZ]	1303 [PPRZ· s]
ang. rate damper P=300	6.08 [deg]	349 [PPRZ]	1303 [PPRZ· s]
ang. rate damper P=400	5.92 [deg]	339 [PPRZ]	1303 [PPRZ· s]
ang. rate damper P=450	5.84 [deg]	333 [PPRZ]	1303 [PPRZ· s]
2INDI	5.88 [deg]	346 [PPRZ]	1303 [PPRZ· s]

Table 6.4: 2INDI damper - disturbance

Additional Figures

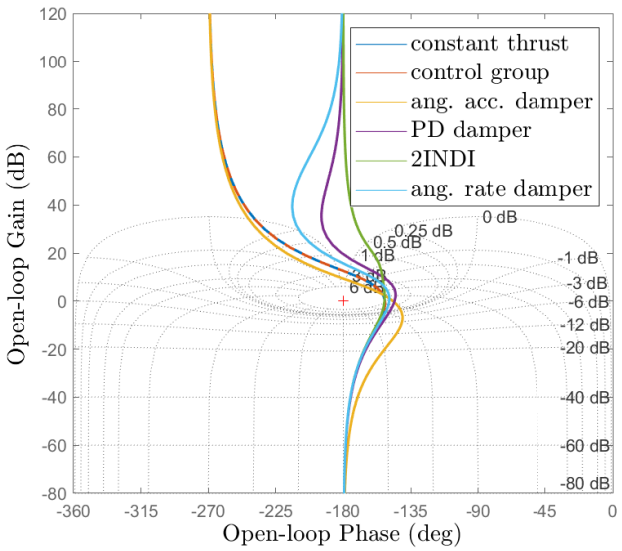

Figure 6.5: Nichols plot for all the investigated strategies.

IV

Conclusion

7

conclusion and recommendations

To conclude, let's recall the research question from the Introduction:

How can a rigidly interconnected flying vehicle be controlled without communication between them and with the possibility of in-flight disassembly?

First, the physical platform was to be designed and built. Chapter 2 provided information for the physical properties of different kinds of aircraft, including a multirotor and the VTOL biplane. Chapter 4 and 4.4 showed different types of Cooperative aircraft and how they can be released in-flight in some cases. However, given the requirement of both endurance and manoeuvrability, the literature review showed a knowledge gap here. The Scientific Article proposes a novel combination of a quadrotor and a biplane that meets the requirements set in the Introduction. In-air disassembly is possible using a pin release system located in the motor mounts of the quadrotor. The successful tests of the in-flight release state that this is a feasible option for at least the hover phase. Experiments in forward flight and considering the endurance are yet to be performed. Also, the biplane's role as a data relay station remains to be developed.

Second, challenges considering the joint control strategy have been addressed in this report. From the different available attitude controller methods, INDI was chosen as the primary controller type. Especially for hybrid aircraft susceptible to disturbances, INDI has proven to be a well-performing and robust controller. Generally, with any form of cooperative flight, some form of communication is used. Since the quadrotor and the biplane have no intercommunication, this meant another knowledge gap. Having no intercommunication means that the quadrotor is limited from a measurement and a reference state point of view. The biplane is given full knowledge of the reference states and has a full attitude INDI controller. For the quadrotor, different control strategies have been simulated and tested. An angular rate damper strategy has proven to perform the best in both simulation and practical verification. Using proportional control, this angular rate damper strategy tries to counteract all angular rate movements it detects. The flight performance was significantly improved for disturbance rejection while having a minimal decrease in intentional attitude changes, as shown in the Scientific article. Also, the least amount of energy and peak input command were required for the step input response and step disturbance rejection. This proved that using a proportional control angular rate damper controller alongside a full INDI attitude controller is feasible as a joint control strategy, answering the second part of the research aim. Future research should include testing for the full flight envelope, and also outer loop control needs to be implemented to have full autonomous capability of this aircraft.

Bibliography

[1] R. Dahiya and A. Singh, "Theoretical and simulation based approach for controlling aircraft longitudinal and lateral yaw damper movement using pid controller," 2017.

[2] C. De Wagter, B. Remes, E. Smeur, F. van Tienen, R. Ruijsink, K. van Hecke, and E. van der Horst, "The nederdrone: A hybrid lift, hybrid energy hydrogen uav," *international journal of hydrogen energy*, vol. 46, no. 29, pp. 16003–16018, 2021.

[3] Orzetto, "A typical, single-input, single-output feedback loop with descriptions for its various parts.." `https://commons.wikimedia.org/wiki/File:Feedback_loop_with_descriptions.svg`.

[4] E. Smeur, *Incremental Control of Hybrid Micro Air Vehicles*. PhD thesis, Delft University of Technology, 2018.

[5] U. S. A. Force, "North american xp-82 twin mustang 44-83887 on test flight over sierras, 1945.." `https://commons.wikimedia.org/wiki/File:Feedback_loop_with_descriptions.svg`, 1945.

[6] M. A. Dehghani and M. B. Menhaj, "Communication free leader-follower formation control of unmanned aircraft systems," *Robotics and Autonomous Systems*, vol. 80, pp. 69–75, 2016.

[7] S. M. Ross, "Formation flight control for aerial refueling," 2006.

[8] Code7700, "Amateur test pilot." `https://www.code7700.com/amateur_test_pilot.htm`, 2021. (Accessed: 2021-07-05).

[9] D. B. Wilson, A. Göktogan, and S. Sukkarieh, "Guidance and navigation for uav airborne docking.," in *Robotics: Science and Systems*, vol. 3, 2015.

[10] R. Oung and R. D'Andrea, "The distributed flight array: Design, implementation, and analysis of a modular vertical take-off and landing vehicle," *The International Journal of Robotics Research*, vol. 33, no. 3, pp. 375–400, 2014.

[11] D. Saldana, B. Gabrich, G. Li, M. Yim, and V. Kumar, "Modquad: The flying modular structure that self-assembles in midair," in *2018 IEEE International Conference on Robotics and Automation (ICRA)*, pp. 691–698, IEEE, 2018.

[12] D. Saldana, P. M. Gupta, and V. Kumar, "Design and control of aerial modules for inflight self-disassembly," *IEEE Robotics and Automation Letters*, vol. 4, no. 4, pp. 3410–3417, 2019.

[13] T. Technics, "Helicopter flight control." `https://www.thaitechnics.com/helicopter/heli_control.html`, 2007. (Accessed: 2021-07-04).

[14] J. Zhang, Z. Ren, C. Deng, and B. Wen, "Adaptive fuzzy global sliding mode control for trajectory tracking of quadrotor uavs," *Nonlinear Dynamics*, vol. 97, no. 1, pp. 609–627, 2019.

[15] T. Luukkonen, "Modelling and control of quadcopter," *Independent research project in applied mathematics, Espoo*, vol. 22, p. 22, 2011.

[16] T. S. Lembono, J. E. Low, L. S. T. Win, S. Foong, and U.-X. Tan, "Orientation filter and angular rates estimation in monocopter using accelerometers and magnetometer with the extended kalman filter," in *2017 IEEE International Conference on Robotics and Automation (ICRA)*, pp. 4537–4543, IEEE, 2017.

[17] Y. Ma, Z. Cai, N. Liu, and Y. Wang, "System composition and longitudinal motion control simulation of vehicular towed autogyro," in *2016 IEEE Chinese Guidance, Navigation and Control Conference (CGNCC)*, pp. 1018–1023, IEEE, 2016.

[18] J. Aletky, "Out of the black: Slt vtol uav." `https://diydrones.com/profiles/blogs/out-of-the-black-slt-vtol-uav`, 2014. (Accessed: 2021-07-01).

[19] B. Allen, "Ten-engine electric plane completes successful flight test." `https://www.nasa.gov/langley/ten-engine-electric-plane-completes-successful-flight-test`, 2017. (Accessed: 2021-07-01).

[20] E. J. Smeur, M. Bronz, and G. De Croon, "Incremental control and guidance of hybrid aircraft applied to the cyclone tailsitter uav," *arXiv preprint arXiv:1802.00714*, 2018.

[21] A. S. Saeed, A. B. Younes, C. Cai, and G. Cai, "A survey of hybrid unmanned aerial vehicles," *Progress in Aerospace Sciences*, vol. 98, pp. 91–105, 2018.

[22] H. Gu, X. Lyu, Z. Li, S. Shen, and F. Zhang, "Development and experimental verification of a hybrid vertical take-off and landing (vtol) unmanned aerial vehicle (uav)," in *2017 International Conference on Unmanned Aircraft Systems (ICUAS)*, pp. 160–169, IEEE, 2017.

[23] P. Hartmann, C. Meyer, and D. Moormann, "Unified velocity control and flight state transition of unmanned tilt-wing aircraft," *Journal of guidance, control, and dynamics*, vol. 40, no. 6, pp. 1348–1359, 2017.

[24] J. M. Beach, M. E. Argyle, T. W. McLain, R. W. Beard, and S. Morris, "Tailsitter attitude control using resolved tilt-twist," in *2014 International Conference on Unmanned Aircraft Systems (ICUAS)*, pp. 768–779, IEEE, 2014.

[25] B. Theys, C. Notteboom, M. Hochstenbach, and J. De Schutter, "Design and control of an unmanned aerial vehicle for autonomous parcel delivery with transition from vertical take-off to forward flight," *International Journal of Micro Air Vehicles*, vol. 7, no. 4, pp. 395–405, 2015.

[26] M. Cunningham and J. E. Hubbard, "Open loop system identification of a small multirotor vehicle with an active feedback control system," in *2018 Atmospheric Flight Mechanics Conference*, p. 3475, 2018.

[27] H.-B. Shin and J.-G. Park, "Anti-windup pid controller with integral state predictor for variable-speed motor drives," *IEEE Transactions on Industrial Electronics*, vol. 59, no. 3, pp. 1509–1516, 2011.

[28] F. Zhanqi and L. L. Xi'an, "The high angle of attack aerodynamic modeling and nonlinear dynamic inversion flight control law design," in *IEEE 10th International Conference on Industrial Informatics*, pp. 901–905, IEEE, 2012.

[29] C. Miller, "Nonlinear dynamic inversion baseline control law: architecture and performance predictions," in *AIAA Guidance, Navigation, and Control Conference*, p. 6467, 2011.

[30] S. A. Snell, D. F. Enns, and W. L. Garrard Jr, "Nonlinear inversion flight control for a supermaneuverable aircraft," *Journal of guidance, control, and dynamics*, vol. 15, no. 4, pp. 976–984, 1992.

[31] E. J. Smeur, Q. Chu, and G. C. de Croon, "Adaptive incremental nonlinear dynamic inversion for attitude control of micro air vehicles," *Journal of Guidance, Control, and Dynamics*, vol. 39, no. 3, pp. 450–461, 2016.

[32] S. Sieberling, Q. Chu, and J. Mulder, "Robust flight control using incremental nonlinear dynamic inversion and angular acceleration prediction," *Journal of guidance, control, and dynamics*, vol. 33, no. 6, pp. 1732–1742, 2010.

[33] E. J. Smeur, M. Bronz, and G. C. de Croon, "Incremental control and guidance of hybrid aircraft applied to a tailsitter unmanned air vehicle," *Journal of Guidance, Control, and Dynamics*, vol. 43, no. 2, pp. 274–287, 2020.

[34] E. J. Smeur, G. C. de Croon, and Q. Chu, “Cascaded incremental nonlinear dynamic inversion for mav disturbance rejection,” *Control Engineering Practice*, vol. 73, pp. 79–90, 2018.

[35] C. Cheron, A. Dennis, V. Semerjyan, and Y. Chen, “A multifunctional hil testbed for multirotor vtol uav actuator,” in *Proceedings of 2010 IEEE/ASME International Conference on Mechatronic and Embedded Systems and Applications*, pp. 44–48, IEEE, 2010.

[36] E. Fresk and G. Nikolakopoulos, “Full quaternion based attitude control for a quadrotor,” in *2013 European control conference (ECC)*, pp. 3864–3869, IEEE, 2013.

[37] E. Smeur, D. Höppener, and C. De Wagter, “Prioritized control allocation for quadrotors subject to saturation,” in *International Micro Air Vehicle Conference and Flight Competition*, no. September, pp. 37–43, 2017.

[38] Ardupilot, “Ardupilot documentation.” `https://ardupilot.org/ardupilot/#`.

[39] PaparazziUAV, “Paparazziuav wiki.” `http://wiki.paparazziuav.org/wiki/Main_Page`.

[40] PX4, “Px4 flight modes overview.” `https://docs.px4.io/v1.9.0/en/getting_started/flight_modes.html`, 2021. (Accessed: 2021-12-10).

[41] A. Carey, *Twin Mustang: The North American F-82 at War*. Images of War, Pen & Sword Books Limited, 2014.

[42] Wikipedia, “Twin fuselage aircraft.” `https://en.wikipedia.org/wiki/Twin-fuselage_aircraft`, 2021. (Accessed: 2021-12-10).

[43] R. Duivenvoorden, M. Voskuijl, L. Morée, R. N. A. Force, J. de Vries, and F. van der Veen, “Numerical and experimental investigation into the aerodynamic benefits of rotorcraft formation flight,” in *Vertical Flight Society’s 76th Annual Forum and Technology Display*, 2020.

[44] C. der Kleij, “Close formation flight control- with application in commercial aviation.” `http://resolver.tudelft.nl/uuid:eaab3e0d-f836-49ca-902d-1a62b0997012`.

[45] D. Douxchamps, S. Lugan, Y. Verschueren, L. Mutuel, B. Macq, and K. Chihara, “On-board axial detection of wake vortices using a 2-m m lidar,” *IEEE Transactions on Aerospace and Electronic systems*, vol. 44, no. 4, pp. 1276–1290, 2008.

[46] NATO, “Air to air refuelling manual,” p. 67, 2000.

[47] Z. Gosiewski and L. Ambroziak, “Formation flight control scheme for unmanned aerial vehicles,” in *Robot Motion and Control 2011* (K. Kozłowski, ed.), (London), pp. 331–340, Springer London, 2012.

[48] M. Morgan, “A study in drag reduction of close formation flight accounting for flight control trim positions and dissimilar formations,” 2012.

[49] M. Brodecki and K. Subbarao, “Autonomous formation flight control system using in-flight sweet-spot estimation,” *Journal of Guidance, Control, and Dynamics*, vol. 38, no. 6, pp. 1083–1096, 2015.

[50] C. Hanson, J. Ryan, M. Allen, and S. Jacobson, “An overview of flight test results for a formation flight autopilot,” in *AIAA Guidance, Navigation, and Control Conference and Exhibit*, p. 4755, 2002.

[51] A. Mahmood and Y. Kim, “Decentrailized formation flight control of quadcopters using robust feedback linearization,” *Journal of the Franklin Institute*, vol. 354, no. 2, pp. 852–871, 2017.

[52] A. Benallegue, A. Mokhtari, and L. Fridman, “High-order sliding-mode observer for a quadrotor uav,” *International Journal of Robust and Nonlinear Control: IFAC-Affiliated Journal*, vol. 18, no. 4-5, pp. 427–440, 2008.

[53] R. Xue and G. Cai, “Formation flight control of multi-uav system with communication constraints,” *Journal of aerospace technology and management*, vol. 8, no. 2, pp. 203–210, 2016.

[54] W. Ren, “Consensus strategies for cooperative control of vehicle formations,” *IET Control Theory & Applications*, vol. 1, no. 2, pp. 505–512, 2007.

[55] J. Seo, C. Ahn, and Y. Kim, “Controller design for uav formation flight using consensus based decentralized approach,” in *AIAA Infotech@ Aerospace Conference and AIAA Unmanned... Unlimited Conference*, p. 1826, 2009.

[56] Z. Chao, S.-L. Zhou, L. Ming, and W.-G. Zhang, “Uav formation flight based on nonlinear model predictive control,” *Mathematical Problems in Engineering*, vol. 2012, 2012.

[57] M. Turpin, N. Michael, and V. Kumar, “Trajectory design and control for aggressive formation flight with quadrotors,” *Autonomous Robots*, vol. 33, no. 1, pp. 143–156, 2012.

[58] T. S. Tao and R. J. Hansman, “Development of an in-flight-deployable micro-uav,” in *54th AIAA Aerospace Sciences Meeting*, p. 1742, 2016.

[59] A. Bouman, P. Nadan, M. Anderson, D. Pastor, J. Izraelevitz, J. Burdick, and B. Kennedy, “Design and autonomous stabilization of a ballistically-launched multirotor,” in *2020 IEEE International Conference on Robotics and Automation (ICRA)*, pp. 8511–8517, IEEE, 2020.

[60] K. Mizokami, “Black hawk helicopters can now launch drones from midair.” https://www.popularmechanics.com/military/weapons/a32617628/black-hawk-drones/, 2020. (Accessed: 2021-03-08).

[61] C. Jee, “Darpa is testing drones it can launch from a plane—then collect mid-air.” https://www.technologyreview.com/2020/01/31/304849/darpa-is-testing-drone-swarms-it-can-launch-from-a-planethen-collect-mid-air/, 2020. (Accessed: 2021-03-04).

[62] G. Turnbull, “The navy plans to test its new electronic warfare drones this fall.” https://www.c4isrnet.com/electronic-warfare/2019/02/19/the-navy-plans-to-test-its-new-electronic-warfare-drones-this-fall/, 2019. (Accessed: 2021-03-05).

[63] A. Technology, “Altius-600 small unmanned aircraft system.” https://www.airforce-technology.com/projects/altius-600-small-unmanned-aircraft-system/, 2021. (Accessed: 2021-07-01).

[64] S. Jo, B. Lee, J. Oh, J. Song, C. Lee, S. Kim, and J. Suk, “Experimental study of in-flight deployment of a multicopter from a fixed-wing uav,” *International Journal of Aeronautical and Space Sciences*, vol. 20, no. 3, pp. 697–709, 2019.

[65] sUAS News, “Flying launch and recovery system: A true game-changer.” https://www.suasnews.com/2016/06/flying-launch-recovery-system-true-game-changer/, 2016. (Accessed: 2021-03-03).